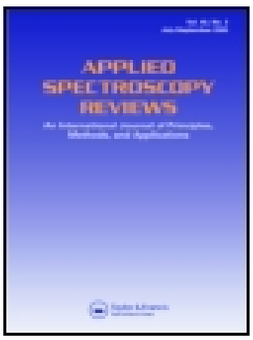

Applied Spectroscopy Reviews

ISSN: 0570-4928 (Print) 1520-569X (Online) Journal homepage: https://www.tandfonline.com/loi/laps20

Raman spectroscopy of breast cancer

Daniela Lazaro-Pacheco, Abeer M. Shaaban, Shazza Rehman & Ihteshamur Rehman

To cite this article: Daniela Lazaro-Pacheco, Abeer M. Shaaban, Shazza Rehman & Ihteshamur Rehman (2019): Raman spectroscopy of breast cancer, Applied Spectroscopy Reviews, DOI: 10.1080/05704928.2019.1601105

To link to this article: https://doi.org/10.1080/05704928.2019.1601105

Published online: 23 Apr 2019.

APPLIED SPECTROSCOPY REVIEWS
https://doi.org/10.1080/05704928.2019.1601105

Taylor & Francis
Taylor & Francis Group

REVIEW

Raman spectroscopy of breast cancer

Daniela Lazaro-Pacheco[a], Abeer M. Shaaban[b], Shazza Rehman[c], and Ihteshamur Rehman[d]

[a]Department of Materials Sciences and Engineering, Kroto Research Institute, North Campus, University of Sheffield, Sheffield, UK; [b]Department of Histopathology, University Hospitals Birmingham NHS Foundation Trust, Queen Elizabeth Hospital Birmingham, and University of Birmingham, Edgbaston, Birmingham, UK; [c]Department of Medical Oncology, Airedale NHS Foundation Trust, Airedale General Hospital, Steeton, West Yorkshire, UK; [d]Engineering Department, Lancaster University, Lancaster, UK

ABSTRACT

Use of spectroscopy for the analysis of biological molecules has significantly increased during the past few years, hence, it is important to accumulate relevant Raman spectroscopic data of breast cancer in one reference document, which will enhance understanding of this field and assist researchers in using Raman spectroscopy to study normal, abnormal, and cancerous breast tissue more precisely and accurately. This article reviews some of the most recent and relevant research work on breast cancer and normal breast tissues analysis using Raman spectroscopy. This review summarizes the differences in frequencies of spectral peak assignments associated with normal and cancerous breast tissues. The aim of this study is to provide an analytical and detailed review including the use of Raman spectroscopy as a tool capable of diagnosis and monitoring of the progression of disease, identifying the chemical pathway of breast cancer, and biomarker identification.

KEYWORDS

Raman spectroscopy; normal breast tissue; breast cancer; pathology; chemical pathway

Aim of this study

During the past few years, the application of vibrational spectroscopy techniques has increased significantly in cancer research. Diagnosis, identification of biomarkers, and the tracking of the progression of breast cancer are major areas of interest within the field of medical research. Recently, a considerable literature has emerged on the evaluation of breast tissue with spectroscopy. This paper reviews recent literature in breast cancer research with Raman spectroscopy and identifies the gaps that remain as research opportunities. This work presents the latest advances in breast cancer research with Raman spectroscopy, and offers a relevant database of the normal, benign and malignant breast tissue spectral bands. This paper will be of significant value to new researchers exploring the use of vibrational spectroscopy to study breast cancer and help in understanding the chemical pathway to the progression of disease.

CONTACT Ihteshamur Rehman i.u.rehman@lancaster.ac.uk Engineering Department, Lancaster University, Lancaster, UK.

Color versions of one or more of the figures in the article can be found online at www.tandfonline.com/laps.

Introduction

Breast cancer represents the most common cancer among women. In 2018, approximately 2 million new cases were diagnosed worldwide (1). Breast cancer cases have increased around the globe in the past decades, but the higher occurrence is reported in developed regions. However, higher mortality rates are registered in less developed countries (2–6). The disease was responsible for 570,000 deaths worldwide in 2015 (7). It is estimated that nearly 2 million new cases will be diagnosed by 2020. Statistics highlight the importance not only of early detection but also the understanding of the chemical pathways of the disease (8–14). In the past decades, Raman spectroscopy has attracted a considerable attention in cancer research. This is due to its potential to provide diagnostic information facilitating the prediction of biochemical progression (15–18). This vibrational technique is based on the Raman inelastic scattering of photons once electromagnetic energy is applied in the near-IR, visible or near-UV spectrum. The difference in frequency between the incident and the Raman-scattered light is known as a Raman shift. This shift is specific to each individual molecule; therefore, the Raman spectrum serves as a fingerprint. Due to this specificity, Raman spectroscopy allows chemical characterization by identifying the chemical bonds and functional groups. Raman spectroscopy is a nondestructive and noninvasive technique with high chemical specificity and sensitivity, requiring minimal sample preparation. These advantages make Raman spectroscopy a powerful and suitable technique for cancer research (19–21).

The use of both the Infrared and Raman microspectroscopy is now widely accepted by both the clinical and research communities and their use is rapidly increasing with the advance in instrumentation and understanding/interpretation of spectra of breast cancer tissues. Primary focus of these studies include:

- Diagnosis by distinguishing between healthy and cancerous tissue, grade and stage of the disease.
- Identification of breast cancer biomarkers, increasing the understanding of breast cancer pathways.
- Cancer progression studies

Therefore, this article presents a review of recent research on breast cancer using Raman spectroscopy. Previous research is summarized and, the advantages and limitations of the proposed methods used to date are reviewed.

Breast and breast cancer

In women, several changes in the mammary gland occur before, during, and after pregnancy, nursing and menopause. The mammary gland development occurs during pregnancy, preparing the breast for milk production, followed by the gland atrophy once nursing is ceased (22). The terminal duct is responsible for draining the lobule. Lobules are the milk-producing glands. Each lobe can host up to 40 lobules, which are arranged in a grapelike cluster form. The terminal duct lobular unit (TDLU) is formed by a lobule and a matching terminal duct. Owing to secretory changes in the epithelial cells and

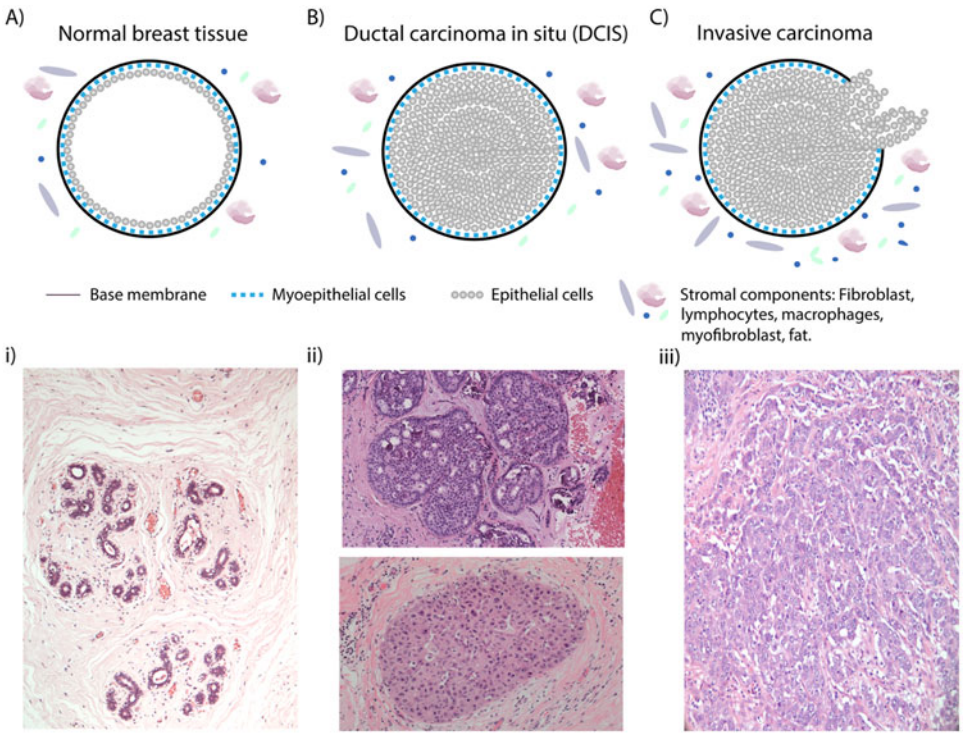

Figure 1. (A) Normal breast tissue, (i) Normal breast tissue H&E 20X (B) Ductal carcinoma in situ, (ii) Breast carcinoma *in situ* low (upper) and high grade (lower) H&E 20X (C) Invasive carcinoma, (iii) Invasive carcinoma H&E 20X: note the infiltration of cancerous cells into the stroma.

lobules in the TDLU, most diseases arise in this area. Tissues that goes through several changes, such as epithelial tissue, have a higher incidence of cancer development. Breast carcinomas comprise the cancer cases developed in the breast epithelial tissue while adenocarcinomas include all the cancer cases started in glandules which are secreting vessels (23).

Carcinogenesis is a multistage process in which cancer develops. In this process, several cell alterations such as apoptosis evasion, insensitivity to anti-growth signals, sustained angiogenesis, self-sufficiency ingrowth signals, limitless replicative potential and tissue invasion and metastasis occur to promote and ensure the growth of a neoplasm (24).

Tumors are formed by cells with abnormal characteristics and can be classified as benign or malignant. Benign tumors are formed by abnormal cells, however, there are not identified as cancerous. By contrast, the malignant tumors are formed by cancer cells. When the cancerous cells are limited to the tissue where they began the tumor is known as *in situ*. The cancerous process is considered invasive once the cancer cells spread within the tissue. Afterwards, epithelial cancer cells can travel through blood vessels and the lymphatic system causing secondary tumors. This process is known as metastasis. Figure 1 shows the subdivision of breast tumors according to its non-invasive and invasive nature using a schematic representation of cancer in terms of cell components and representative histological images.

Table 1. Classification of malignant lesions according to the Royal College of Pathologist guidelines use in the UK.

Malignant noninvasive lesions	Invasive carcinoma
Ductal carcinoma in situ (DCIS)	Pure special type
Rarer subtypes of DCIS	Invasive carcinoma of no special type (NST)
Apocrine DCIS	Mixed invasive tumor
Clear cell DCIS	Carcinoma with apocrine differentiation
Signet ring DCIS	Carcinoma with neuroendocrine differentiation
Neuroendocrine DCIS	Salivary gland type tumors
Cystic hypersecretory DCIS and mucocoele-like DCIS	Secretory carcinoma
DCIS in papilloma, papillary carcinoma in situ and encysted papillary carcinoma	Other malignant tumor: Non-epithelial tumors and secondary malignancies
Paget's disease of the nipple	
Microinvasive carcinoma	

Breast cancer is considered a highly heterogeneous disease as it can be presented in several types and subtypes. The WHO recognized more than 100 types of breast tumors. In the UK, a simplified and more relevant classification by the Royal College of Pathologists is used. A summary of the most common tumor types is shown in Table 1 (25). In addition, a range of subtypes depending on immunochemistry or molecular profiling classification exist. In clinic, breast cancer subtypes are identified scoring for estrogen receptor (ER) using immunochemistry methods (IHC), and Human epidermal growth factor 2 (HER2) protein overexpression identified either with immunohistochemistry or Fluorescence In Situ Hybridization test (FISH). The progesterone receptor (PR) can also be assessed, but it is not compulsory. Assessing the biomarker receptor status is an important task not only to provide an accurate diagnostic but also to offer the best treatment possible. Subtypes based on IHC/FISH classification are shown in Table 2 (26).

Traditional breast cancer diagnosis

The current gold standard for breast cancer screening is by triple assessment using imaging (a combination of X-ray mammography and ultrasound), clinical examination and histological assessment. The use of magnetic resonance imaging (MRI) is limited due to its cost (27). Once a tumor is detected and suspected to be cancerous, a core biopsy procedure is recommended. Needle core biopsy is the standard sampling method. The major drawbacks of needle techniques are the retrieval of insufficient material to assess and sampling error, which results in false negatives. Surgical biopsy can overcome the limitations of needle approaches, but the idea of an open surgery to retrieve whole tissue sections brings its own limitations and possible complications.

Histopathological assessment

Once retrieved, the surgical or needle biopsy is assessed by microscopic evaluation. The histopathological assessment aims to determine the presence and type of cancer. The assessment includes the histoprognostic index, histological parameters, and molecular profile. This report helps to decide the treatment approach. Tumor staging and grading are also required as part of this assessment. The stage is a number representative of the spreading of the tumor and is based on the TNM system. This approach includes the

Table 2. Subtype classification based on immunohistochemical expression of hormone receptors, HER2, proliferation marker ki67 and basal cytokeratins

Subtype	Features
Luminal A	(ER+ /PR+ & Ki-67 $<$ 14%)
Luminal B	(ER+ /PR+ & Ki-67 $\geq$ 14%)
Luminal/HER2	(ER+/PR+/HER2+)
HER2 enriched	(ER−/PR−/HER2+)
Basal-like	(ER−/PR−/HER2− & EGFR + and/or CK5/6 +)
Triple-negative (TN)	(ER−/PR−/HER2− & EGFR− & CK5/6 −)

assessment of three different features: T for Primary Tumor, N for Regional Lymph Nodes, and M for Distant Metastasis. Four stages of breast cancer are possible, with stage 1 being the earliest state of malignancy and stage 4 being metastatic. On the other hand, grading reflects the dedifferentiation degree, and histological and cytological criteria are used. Therefore, the grade score is a number that indicates the tumor morphology and its proliferative capacity. Three tumor grades are possible with one being the lowest or well-differentiated, and three the highest, poorly differentiated and most aggressive (28, 29).

Challenges in diagnosis and monitoring breast cancer

Rapid and reliable tumor detection techniques, rather than a complete diagnosis tool have been used for cancer detection. The majority of these techniques is based on the differences in the properties between cancerous and healthy tissue, usually electric or electromagnetic. However, tumor detection techniques are not able to offer a complete diagnosis regarding the type, stage, and classification of the disease.

On the other hand, the current histopathological assessment presents limitations. IHC assays can present intra- and inter-laboratory variations when the ER is assessed. These variations are due to discrepancies among methods, fixation, staining, and antigen retrieval. For example, a short fixation time can result in a false negative in the ER status. Besides, the pathologist training and experience might cause inter-laboratory variations. In a study conducted by Pusztai et al., the concordance level in different laboratories for ER and HER2 showed variations. For example, the quantification of HER2 expression using FISH reached only 85% of concordance (30).

Genomic profiling has been proposed to understand the cancer progression and offer a clearer significant classification. Moreover, the biggest drawback for molecular subtyping is the lack of standardized and high-throughput protocols and data processing. In addition, the reproducibility, cost, and training must be improved before considering bringing molecular profiling into clinical diagnosis (26, 30–32).

Raman spectroscopy

Vibrational spectroscopy has demonstrated its potential to provide diagnostic information. Additionally, vibrational spectroscopy can facilitate the prediction of the biochemical progression for different diseases in a rapid nondestructive manner.

The interaction of electromagnetic energy, near-IR or visible or near-UV, with the electron cloud of a sample excites the vibrational states. Once the molecule relaxes, it

Table 3. Raman spectral assignments for breast tissue.

Peak (cm^{-1})	Assignment	
3067	Nucleic acids/proteins C–H aromatic	(88)
3009	Lipids, C–H stretching	(88)
2959	CH_3 (asymmetric CH_3 stretch of lipids, DNA, and proteins)	(80)
2940	C-H stretching, aromatic and aliphatic amino acids, charged amino acids, proline, threonine, histidine, lipids, proteins	(89)
2930	CH2 (asymmetric CH_2 stretch of lipids)	(80)
2926	Saturated bonds of lipids, fatty acids and polypeptide proteins. CH_2 antisymmetric stretching	(89)
2880	CH2 (asymmetric CH_2 stretch of lipids)	(80)
2850	CH2 (symmetric CH_2 stretch of lipids)	(80)
2807	Aliphatic -N-CH3, amine	(90)
1746, 1654, 1440, 1301, 1267, and 1078	Vibrational modes of lipids	(82)
1746	C=O stretch (lipid)	(91)
1660	Fatty acids of the adipose tissue. C=C stretching (1660 for cis, 1654 for trans)	(89)
1654–1655	Amide I (C=O stretching mode of proteins, α-helix conformation)/C=C lipid stretch	(91)
1652–1653	Lipid (C=C stretch)	(91)
1632	C-O asymmetric stretching. Calcium oxalate dihydrate-Type I calcification	(92)
1616	C=C stretching mode of tyrosine and tryptophan	(91)
1603	C=C in-plane bending mode of phenylalanine and tyrosine	(91)
1579	Pyrimidine ring (nucleic acids) and heme protein	(91)
1556, 1530, 1083, and 1002	vibrational modes of proteins	(82)
1548	Tryptophan. Amide II, in plane N-H bending	(90, 91)
1520–1538	C=C bond of the polyene chain in carotenoids	(89, 91)
1485	Nucleic acid purine bases (guanine and adenine)	(91)
1477	C-O symmetric stretching. Calcium oxalate dihydrate-Type I calcification	(92)
1446	CH_2 bending mode of proteins. CH_2(overlapping asymmetric CH_3 bending & CH_2 scissoring (is associated with elastin, collagen& phospholipids)	(80, 91)
1443	CH_2 deformation (lipids and proteins)	(91)
1437	CH_2 deformation (lipid)	(91)
1386	CH_3 bend	(91)
1369	Guanine, TRP (protein), porphyrins, lipids	(91)
1336	Polynucleotide chain (DNA–purine bases)	(91)
1335–1345	CH_3CH_2 wagging mode of collagen	(91)
1313	CH_3CH_2 twisting mode of collagen/lipids	(91)
1304	CH_2 deformation (lipid)/adenine, cytosine	(91)
1300	C-H (CH_2) bend. Lipids	(92)
1279	Amide III: α-helix	(91)
1265-1240	Amide III (C–N stretching mode of proteins, indicating mainly α-helix conformation)	(91)
1264	=C–H in plane bending (lipid)	(91)
1260	Amide III: unordered. C–N–H (ν (CN), δ(NH) amide III, α-helix conformation collagen, tryptophan; and $PO2^-$ asymmetric (Phosphate I))	(80, 91)
1258	Amide III/adenine/cytosine	(91)
1243	Amide III: collagen (CH_2 wag, C–N stretch)/ pyrimidine bases (C, T)	(91)
1220–1221	Amide III: β-sheet	(91)
1209	Tryptophan and phenylalanine ν(C–C_6H_5) mode	(91)
1206	Hydoxyproline, tyrosine	(91)
1189	C–C_6H_5 Phe, Trp	(88)
1180–1184	Cytosine, guanine, adenine	(91)
1170	C–H in-plane bending mode of tyrosine	(91)
1155	C–C (& C–N) stretching of proteins and carotenoids	(89, 91)

(*continued*)

Table 3. Continued.

Peak (cm^{-1})	Assignment	
1130	C-C stretch. Lipids	(92)
1123	C–C stretching mode of lipids/protein C–N stretch/glucose	(91)
1117–1119	C–C stretch (breast lipid)	(91)
1096	O-P-O (stretching PO_2^- symmetric (Phosphate II) of phosphodiesters	(80)(90)
1087–1090	C–C stretch, O–P–O − stretch	(91)
1083	C–N stretching mode of proteins (and lipid mode to lesser degree)	(91)
1078	C–C or C–O stretch (lipid), C–C or PO2 stretch (nucleic acids)	(91)
1075	$\nu_3(PO_4)$ Hydroxyapatite- Type II calcification	(92)
1064	Skeletal C–C stretch lipids	(91)
1061-1028	$\nu_3(PO_4)$ Hydroxyapatite- Type II calcification	(92)
1031	C–H in-plane bending mode of phenylalanine	(91)
1004	Phenylalanine. CH_3 rocking coupled with C-C stretching of carotenoids	(89, 92)
1001	Symmetric ring breathing mode of phenylalanine	(91)
968	C-C stretching lipids	(89)
960	$\nu_1(PO_4)$ totally symmetric stretching. Hydroxyapatite- Type II calcification	(92)
957	Hydroxyapatite/carotenoid/cholesterol	(91)
938	C–C stretch backbone	(91)
935	C–C stretching mode of proline and valine and protein backbone (α-helix conformation)/glycogen	(91)
932	Skeletal C–C: α-helix	(91)
920	C–C stretch of proline ring/glucose/lactic acid	(91)
912	C-C stretching. Calcium oxalate dihydrate- Type I calcification	(92)
880	Lipids/carbohydrates/collagen	(88)
877	Tryptophan, proteins. Antisymmetric stretching in phosphatidylcholine, lipids	(89)
869	Proline	(91)
859	Tyrosine/collagen	(91)
853	Ring breathing mode of tyrosine and C–C stretch of proline ring	(91)
842	Glucose	(91)
828	Out of plane ring breathing tyrosine/O–P–O stretch DNA	(91)
826	O–P–O stretch (DNA)	(91)
786	DNA: O-P-O cytosine, uracil, thymine	(91)
781	Cytosine/uracil ring breathing (nucleotide)	(91)
780	C–C (C–C stretch of proline, hydroxyproline and tyrosine and ν_2 PO_2^- stretch of nucleic acids bands)	(80)
759	Tryptophan	(91)
755	Symmetric breathing of tryptophan	(91)
727	$N^+(CH_3)_3$ symmetric stretching of phosphatidylcholine lipids	(89)
726	C–S (protein)/CH2 rocking (phospolipids)/adenine	(91)
717–719	C–N (membrane phospholipid head)/adenine	(91)
679	Guanine ring breathing	(91)
676	ν (δ (CCN)), Vinyl & Porphyrin mode	(90)
669	C–S stretching mode of cystine	(91)
650	C–C (Symmetric breathing of tryptophan – protein assignment	(80)
643	C–C twisting mode of tyrosine	(91)
621	C–C twisting mode of phenylalanine	(91)
573	Tryptophan/cytosine, guanine	(91)
524	S–S disulfide stretch in proteins	(91)
484–490	Glycogen	(91)

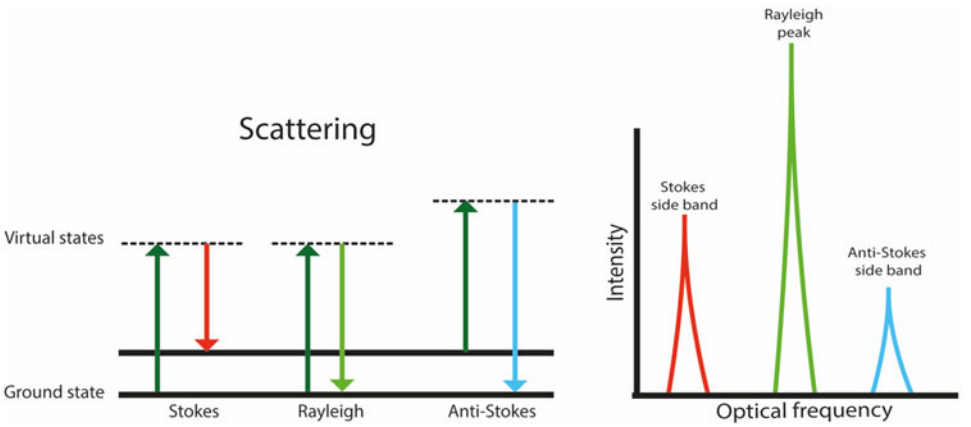

Figure 2. Types of light scattering in terms of energy; maintained (Raleigh), loss due to vibration (Stokes), or gained due to vibration (anti-Stokes), and intensity versus frequency.

emits a photon. Raman spectroscopy focuses on the inelastic scattering of these photons. In the inelastic scattering, the photon's frequency is shifted due to the vibrational excitation. The difference in frequency between the incident and the Raman-scattered lights is known as Raman shift. If the scattered photon is emitted by an electron falling to a higher energy state, it is known as Stokes shift (or red-shifted) and the photon has a lower frequency. On the contrary, if the photon is emitted by an electron falling to a lower energy state, the shift is known as anti-Stokes or blue-shift and the photon has a higher frequency (19). A schematic representation of both shifts is shown in Figure 2. The energy needed to promote the vibrational state change is the difference between the incident and scattered photon. This energy is specific for each individual molecule. Due to this chemical specificity, RS allows the characterization of materials and biological samples.

Raman spectroscopy is a label-free powerful technique with incredible potential in biological analysis. RS is considered less invasive, the sample preparation is minimum or not required, and allows immediate data collection. *In vivo* and *ex vivo* analysis can be performed with special accessories, such as, external fiber optic probes. Additionally, accurate qualitative and quantitative results can be obtained due to the depth and spatial high resolution (16).

The integration of confocal microscopy to Raman systems has allowed the analysis of small volumes, in particular depth profiling of biological samples. A diagram and brief explanation of confocal Raman spectroscopy is shown in Figure 3.

Spectroscopic techniques involve several variables, and consequently produce multivariate data. Obtaining information using approaches such as Consider One Separate variable at a Time (COST) is not effective for accurate and efficient analysis (33). Therefore, chemometric and multivariate analysis are preferred. Chemometrics involve a combination of statistical and mathematical analysis on chemical data to extract information. Due to the size of the data sets, chemometrics requires computationally intensive methods (34). Multivariate analysis aims to reduce data. This aim is driven by the large number of values, for example, thousands of intensity values (35).

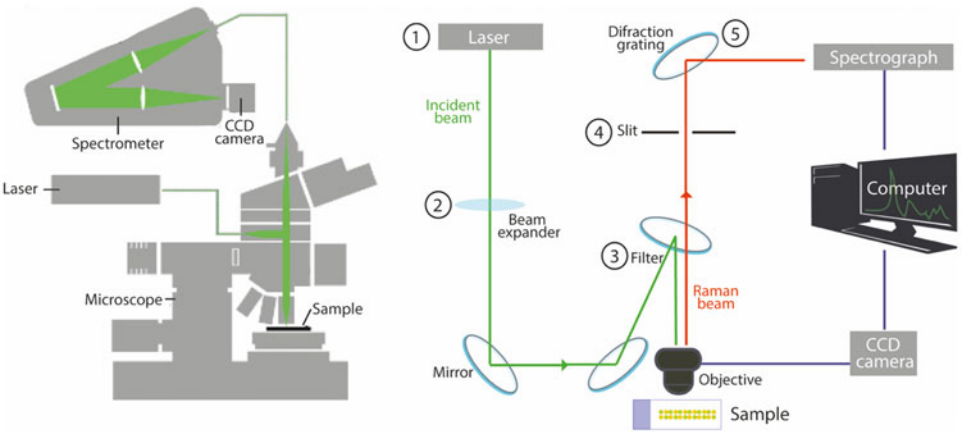

Figure 3. Schematic representation of a confocal Raman microscope. This is a representation of the incident beam coming from the laser 1) and being expanded (2). After this, the laser goes through mirrors and optical arrangements to pass through a filter (3) before arriving to the objective and interacting with the sample. The inelastic Raman scattering is collected though the objective and passed through the filter. Once there it is sent through a slit (4) to the grating (5) before arriving to the spectrograph. Once in the spectrograph the beam is imaged. (Adapted from Rehman et al., 2013 and Dieing et al., 2011) (19, 52).

Multivariate analysis comprises two types of algorithms: supervised and unsupervised. Unsupervised algorithms are exploration processes without prior expectations. As a result of this, clusters and gradients can be identified, which provides information on chemical differences and similarities (36). Unsupervised algorithms can assist in identifying patterns, trends and detect outliers. Principal component analysis (PCA), Cluster analysis (CA), k-means, hierarchical cluster analysis (HCA), and neural networks are examples of this type of algorithm.

Supervised algorithms are usually applied to data sets for validation because the classification is known before the analysis. Linear discriminant analysis (LDA), partial least squares discriminant analysis (PLS-DA), support vector machine (SVM), and logistic regression are examples of supervised algorithms. The data is manually classified using unique labels. A set of classification rules, known as classifiers, are used to discriminate and separate the data to its maximum capacity and classify any unlabeled data (37, 38).

These methods have been widely used to classify and validate various chemometrical models analyzing different tissues with different spectroscopic techniques (39–51).

Importance of cancer disease progression

In oncology care and research, two important events guide therapy and treatment of cancer, "tumor response" and "disease progression." Tumor response assesses therapy efficacy early in the course of treatment. Disease progression is clinically understood as a growing and spread of cancer representing a failed treatment. This assessment is commonly used to decide if the therapy approach requires modifications and helps to calculate time to progression endpoints in clinical research. Tumor response to therapy in clinical trials can be assessed radiologically using the RECIST Criteria (Response

Evaluation Criteria In Solid Tumors) or histologically using established systems for assessing response such as the Residual Cancer Burden Calculator (53).

In general terms, the tumor progression indicates phenotypic changes. Among these changes, there are specific morphological, molecular, and functional changes. Progression of cancer comprises a wide variety of mechanisms where stroma, angiogenesis, inflammation, immune system, hormones, and xenobiotics play a vital role (54, 55). All these processes and mechanism will cause biochemical changes at tissue level (56–58). Hence, identifying the biochemical changes in cancerous tissue can facilitate the metastatic potential assessment as well as the aggressiveness at different progression time-points (59). In clinical practice, tracking the progress of cancer supports several decisions, such as, changes in therapy.

Breast cancer is the primary source for the majority of cancer deaths in women. However, metastases at distant sites and its complications are the main cause of death. Breast cancer is likely to metastasize to bone, central nervous system and viscera, translating into a poor prognosis and low overall survival (60, 61). Biomarkers are urgently needed to recognize patients at higher metastases risk, in order to tailor treatments strategies, improve clinical management and find new therapeutic targets. This knowledge has the potential to modify the tumor environment, tumorigenesis and cancer stem cells influence (14).

Raman spectroscopy and breast cancer analysis

Biochemical changes in the different tissue components are manifestations of the pathological processes. Embracing this opportunity, the chemical characterization achieved with vibrational spectroscopy can be used to identify the presence of diseases at different stages. This is the case for Raman spectroscopy of breast cancer. The analysis of human and animal tissue indicates that Raman spectroscopy has the potential for non-invasive detection, grading, and classification of breast cancer. Many of the cancerous and precancerous changes originate in the duct and lobules lining; therefore, the use of Raman signatures could facilitate the identification of precancerous lesions and carcinomas *in vivo* (62). The spatial resolution of the Raman spectroscopy techniques allows them to be used in ducts and cellular organelles facilitating its use in diagnosis and disease monitoring (63). Cancer is a multifactorial disease that usually requires the use of imaging biomarkers to monitor several processes, such as, cell proliferation and migration, receptor and gene expression, metabolism, hypoxia, apoptosis, angiogenesis, and signal transduction. One of the main advantages offered by Raman spectroscopy is the label-free analysis of tissue that allows the analysis of samples without using expensive dyes or radionuclides (64–67).

Normal breast and breast cancer differences

There is a significant amount of published studies describing the biochemical fingerprint of breast tissues. The contents of lipids and proteins has been identified as the main differences between normal and malignant breast tissues. Normal breast tissue presents a dominance in Raman bands due to lipids, while malignant lesions exhibit

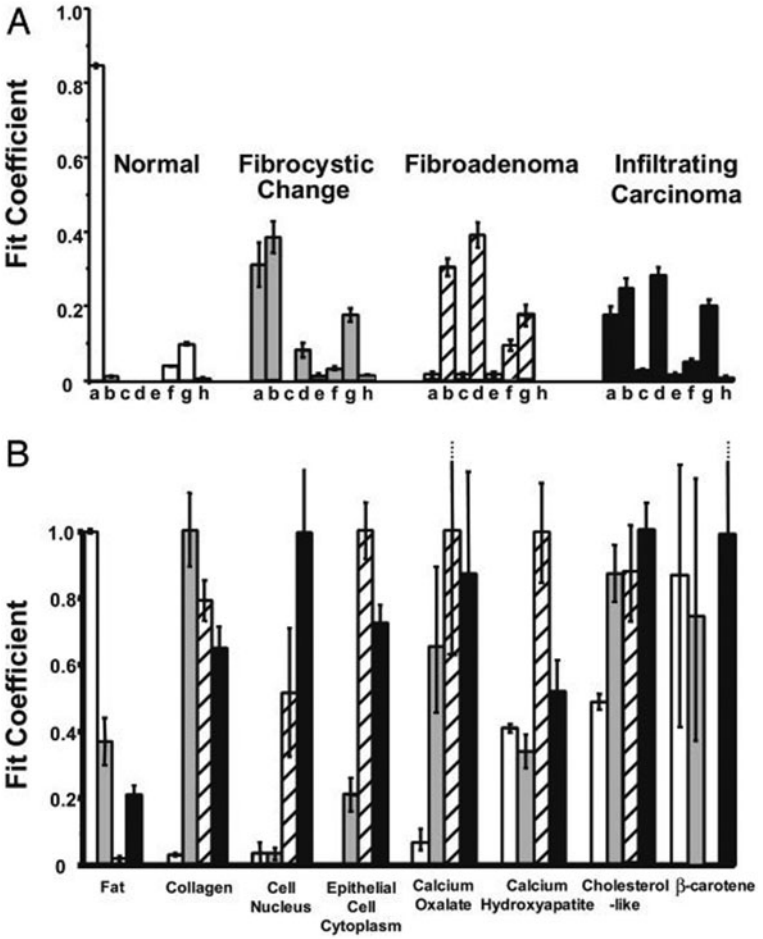

Figure 4. Histograms displaying the average composition of samples diagnosed as normal (white), fibrocystic change (gray), fibroadenoma (striped), and infiltrating carcinoma (black). The one-SD confidence intervals are shown for each model component. (A) Data are grouped according to pathological diagnosis: fat (a), collagen (b), cell nucleus (c), epithelial cell cytoplasm (d), calcium oxalate (e), calcium hydroxyapatite (f), cholesterol-like (g), and ß- carotene (h). (B) Data are clustered by model component, and each histogram cluster is normalized to the largest of the four values (78).

bands associated with proteins (68). A number of authors reported dominance of lipids, especially fatty acids in normal tissue spectra. Whereas, protein dominates abnormal tissue, both benign and malignant (20, 69, 70). Differences in the 2800–3000 cm^{-1} region of the Raman spectrum are associated with variations in the content of lipids and proteins. A higher contribution of proteins can be attributed to; (i) uncontrolled and abnormal cell proliferation, (ii) cell division, and (iii) migration in the malignant tumor (64, 71). Fatty acids such as triolein and oleic acid has been identified as part of the lipid component (72–74). Manoharan et al. had established two simple empirical features to differentiate normal and abnormal breast tissue. This includes the shift to higher frequency, of the CH_2 bending mode from 1445 to ~1450 cm^{-1} and the increase in area of the band located at 1650 cm^{-1} in the normal tissue and its shifted analogue 1667 cm^{-1} in the abnormal tissue (68).

Brożek-Płuska research group analyzed *ex vivo* breast samples without prior preservation treatment. Samples from 44 patients including tumor tissue, healthy tissue and blood vessels were evaluated acquiring 321 spectra. Normal breast tissue presented clear peaks corresponding to stretching of carotenoids and asymmetric vibration of lipids. A spectrum with higher grade of fluorescence and lack of high intensity peaks was obtained for the malignant tissue. The reduced intensity of carotenoids and lipid peaks suggested a lower content of these components in the malignant tissue. The carotenoids reduction was explained through the oxidation of lipofuscin material, and the lipid reduction was attributed to lipid peroxidation (75). All the risk factors and causalities of cancer have not been established with precision. Aging processes, oxidative, and free-radical activity have been proposed as contributors for this disease. Owing to this fact, several studies have focused on these phenomena. Lipofuscin are age-related pigments produced by different biological materials and resulting in fluorophores products. Its involvement in aging processes has been ample investigated (76, 77). The results of Brożek-Płuska's study regarding pigments products open the possibility to suggest that free radical theory of aging could provide useful information about the carcinogenesis process. Oxidation processes are associated with cytotoxic or genotoxic production (75).

Using an optical fiber Raman probe system, breast cancer and other breast diseases such as fibrocystic change, and fibroadenoma were confirmed. Analysis of samples from 58 patients resulted in 94% sensitivity and 96% specificity (78). Haka et al. used the Shafer-Peltier et al. spectroscopic model of breast tissue (79). In this model, cell nucleus, collagen, epithelial cell cytoplasm, fat, β-carotene, calcium hydroxyapatite, calcium oxalate dihydrate, cholesterol-like lipid deposits, and water basis spectra were acquired to compare with the sample's spectra. The basis spectra is given a value of 1 and based on the spectrum of the sample a fraction is calculated. This fraction is known as the fit coefficient and allows a quantitative comparison. Chemical composition was established with them and the fit coefficients signatures are presented in Figure 4. Maximum possible estimation was used to calculate the sample probability of representing a benign or malignant lesion. Normal breast presents a higher fat content while the collagen content increases on all abnormal breast samples. Breast pathologies are known to present a certain scarring degree in which proliferation of fibroblast and collagen production can easily be associated with the study results. Additionally, in invasive carcinoma the cancerous cells promote the proliferation of fibroblasts in stroma. In cancerous and benign tumors, the fit coefficients for nuclei and epithelial cell cytoplasm were high. These numbers suggested abnormal cell proliferation and enlargement of nuclei, which are neoplasm hallmarks. Therefore, nuclear to cytoplasm ratios allowed the differentiation between benign and malignant neoplasm. Furthermore, fat played a role on this differentiation. This role was determined by the cancer cell infiltration into fat and the fat tissue pushing aside once the benign tumors grows. It has been reported that precancerous lesions can be diagnosed by considering the intermediate nuclear-to-cytoplasm ratio (78). Different grades of ductal carcinoma in situ (DCIS) and invasive ductal carcinoma (IDC) were distinguished by Raman spectroscopy using the nuclear spectra (80).

When fit coefficient models distinguish between different breast pathologies, the component's contents lead to its classification. For example, the margins of the fibrocystic

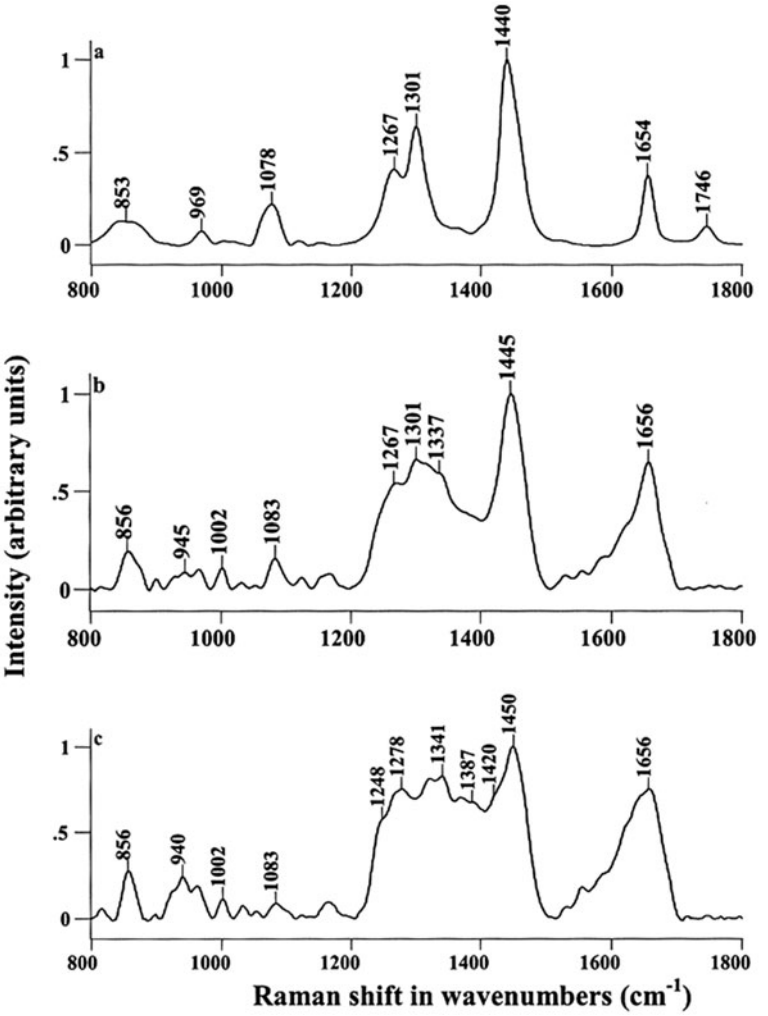

Figure 5. Mean Raman spectra of breast tissues: (a) normal; (b) malignant; (c) benign (82).

samples will present a higher epithelial cell cytoplasm due to fibrosis and adenosis processes. Malignant changes present greater nucleus-to-cytoplasm ratios associated with nuclei enlargement. Additionally, margins of high grade tumors show an increment on the epithelial cell cytoplasm (81). Furthermore, the differences can also be identified with subtraction of the cancerous, benign and normal mean spectra. It has also been reported that the difference between malignant and benign breast tissue was less pronounced in comparison with the normal breast tissue and other breast pathologies (82).

Rehman et al. reported an increase in the intensity of OH, NH and CH spectral peaks, as the grades of the DCIS and IDC increased. This intensity increment can be associated with changes in important biomolecules, such as, nucleic acids, proteins and fatty acids. Peak shifts were also observed in the 1600–600 cm^{-1} region, which were mainly associated with nucleic acid changes. These peak shifts reflect the chemical structural changes and helped with determining different grades. On this research, high nuclear grade (HNG) DCIS presented a higher content of lipids represented by fatty

acids and acylglyceride peaks, while low nuclear grade (LNG) DCIS samples were protein-rich (80). These results support previous findings regarding the presence of fatty acids as energy reservoirs and other biological activities, which will be discussed further (83–86).

Breast tissue spectra and interpretation

The characteristic peaks of breast tissue are well-established from a variety of studies. The discrimination between cancerous, benign and normal breast tissue has been extensively reported, moreover early neoplastic changes have been identified using Raman Spectroscopy. Lymph nodes associated with normal breast tissue share the high lipid content. Cancerous mammary tissue decreased the contribution of lipids, shown by a decrease in the intensity of phospholipids C=O stretch at 1746 cm^{-1} and 1440 cm^{-1} bands. Tissue adjacent to tumors (also called tumor bed) spectra resemble normal tissue data, however subtle changes in the intensity can be appreciated, reflecting chemical signs associated with preneoplastic changes. Breast pathologies that involve destruction of adipose tissue such as mastitis showed a lack of phospholipid peak and a broadening caused by superimposed peaks in the 1200–1500 cm^{-1} region (87).

A protein spectral region between 960 and 800 cm^{-1} and lipid/acylglyceride at 1400 and 1080 cm^{-1} can be distinguished on the breast spectrum. On the cancerous cases a relative decrease on the lipid content and an important contribution of the proteins can be easily distinguished when it is compared to normal breast tissue. The main indication of the protein increase is the amide I bands (80).

When benign and malignant neoplasm had been compared, cancerous tissue presented a higher content of lipids represented by 1082, 1301, 1440 cm^{-1} whereas a dominant presence of proteins at 1033, 1002 cm^{-1} was detected of benign tumors. Additionally, benign tumors presented a ΔCH_2 broad red shifted peak, and strong amide I and III bands. Clear visual differences on the fingerprint spectral region were present in normal, malignant and benign breast as it is shown in Figure 5 (82).

As any other biological tissue, the breast is formed by lipids, proteins, amides, nucleic acids and aminoacids. Therefore, contributions from all these biomolecules are expected at different degrees in the spectral region. Fortunately, specific regions for these molecules can be found in the spectral range with their specific peak assignments. These regions include lipids (3100–2680 cm^{-1}), fingerprint (1800–500 cm^{-1}), amides (1800–1140 cm^{-1}), amide I (1800–1510 cm^{-1}), amide II (1510–1390 cm^{-1}), amide III (1390–1140 cm^{-1}), amino acids, and nucleic acids (980–600 cm^{-1}). In order to facilitate a simple and clear peak assignment, Table 3 comprises important and characteristic Raman bands found in breast tissue.

Assignment of spectral bands is the first step towards characterization and spectral data interpretation. Differences in frequency, shape, and intensity are targeted in this primary analysis. However, when hundreds to thousands of spectra and frequencies are collected, a multivariate analysis is recommended. This analysis is achieved through statistical analysis allowing the identification of differences among samples or finding similarities to support its classification.

The use of micro-spectroscopy for diagnosis offers high objectivity which is assisted by the use of multivariate statistical analysis (82). Several studies handling varying quantities of samples and spectra have reported sensitivity, specificity and accuracy above a reasonable threshold. This supports the idea of integrating Raman spectroscopy as a complementary technique in breast cancer diagnosis. For example, Brożek-Płuska et al. achieved principal component analysis (PCA) classification of normal, malignant and benign tissue. The discrimination of breast tissue and its nature was accomplished with 72% sensitivity for cancerous tissue and 62% for benign tumor tissue, with a specificity of 83% for normal tissue (75). In a prospective analysis, Haka et al. validated characteristic algorithm for malignant, benign, and normal breast tissue differentiation with a sensitivity of 83%, and a specificity of 93% (93). The first study reached 94% sensitivity and 96% specificity (78). When the same model was applied to *in vivo* margin assessment an accuracy of 93.3% was achieved (81).

Chemical pathway and disease progression

Frank et al. (69) analyzed human breast biopsies fixed with formalin. Their research was mainly focused on the parameter optimization for Raman spectra acquisition. The reduction of fluorescence was achieved using white light corrections. Sample handling parameters for the manipulation of biological samples were confirmed. For example, long exposition results on sample desiccation. By working with 45 patient samples, Frank et al. confirmed that fluorescence varied among the samples based on the sample's nature. Additionally, this group observed more bands using near-IR excitation in comparison with visible excitation and regardless the background fluorescence. This study analyzed different lipid standards including: oleic acid methyl ester; linoleic acid methyl ester, linoleic acid methyl ester, and elaidic acid methyl ester to establish the lipid components in normal breast tissue. The results suggested that the lipid component in normal breast tissue was monounsaturated and possessed a *cis* configuration. Moreover, it was identified that the major component of the normal breast lipids was an ester of oleic acid.

Clear differences in the lipid profile of cancerous and normal breast samples were detected in different studies (75, 80, 82, 87, 93–96). When the lipid components were compared to the spectra obtained for the breast samples, a dominance of oleic acid was identified for non-cancerous tissue. Oleic acid and its derivatives are components of glycerides in adipose tissue, which can easily explain its dominance in normal breast tissue. On the other hand, cancerous tissue had a remarkable resemblance with arachidonic acid (AA) (96). The difference with Arachidonic acid AA was the missing band at 3009 cm^{-1} corresponding to C-H attached to C=C. This change suggested a metabolism via cyclooxygenase (COX) enzyme pathway instead via lipoxygenase (LOX) that result in eicosanoids which participate in inflammatory processes (97).

COX catalyzes the production of cyclic compound while the LOX produces noncyclic compounds. Arachidonic acid (AA) precedes eicosanoids and derivatives with a bigger biological activity potential than dihomo-γ-linolenic acid (DGLA) and eicosapentaenoic acid (EPA). Some examples of the mentioned biological activity are the stimulation of

thrombus formation, cell proliferation resulting on tumor growth, and aggressive inflammatory reactions (98–100).

Ductal carcinoma samples were compared against normal breast ducts revealing a different protein/lipid profile. Ducts with cancerous cells showed a higher content in sphingomyelin, and saturated acids; especially palmitic acid and mammaglobin. This change in content varies notably, based on the cancer development and progression. These results suggested that the identification of mammaglobin overexpression can be used as a breast cancer biomarker when ducts are being analyzed (101). When the duct membrane was analyzed an important content of sphingomyelin was found. This component was higher in the cancerous samples suggesting that the stiffness is reduced, facilitating the membrane distortion and deformation, affecting several biomolecules. Additionally, the lipid variation in cancerous ducts changed the membrane fluidity. In addition, it has been hypothesized that this might contribute to the invasive process by releasing a pre-invasive content of saturated fatty acids preparing the ECM. The ECM surrounding the cancerous duct presented peaks suggesting an overproduction of proteins (102).

Among different studies, oleic acid and carotenoids dominated normal breast tissue. Carotenoids have antioxidant properties reducing DNA damage and mutations, in addition to offering immune protection. Carotenoids play an important role in cellular processes; they offer protection against oxidative damage, upregulate connexion junctional communication and avoid the lipid oxidation. Gap junctional communication (GJC) has been suspected to play a role in carcinogenesis. *In vitro* studies showed that carotenoids increase GJC inhibiting carcinogen-initiated fibroblast progression to the transformed state. Normal breast tissue proved to contain a higher amount of carotenoids in comparison with cancerous tissue, acting as a fatty acids reservoir (97). Carotenoids presence in normal breast tissue suggests its role as protection against cancer (103). Normal tissue spectra had similarities with oleic acid, linoleic acid, and docosahexaenoic acid. Furthermore, carotenoids, oleic acid, and docosahexaenoic acid are well-known to play a protective role in breast cancer (98).

The increased content of carotenoids in neoplastic tissue can be associated with the carcinogenic mechanisms. Hormone activity and cell processes are strongly associated with breast cancer and tumor growth. Hormone secretion and cell differentiation is regulated by the gap junction communication (GJC), which is upregulated by carotenoids. When color filters were applied to Raman images, the resulting image with the carotenoid and oleic acid filters were similar, suggesting that the adipose tissue components (fatty acids and triglycerides) supply carotenoids dynamically to the breast (89).

On other hand, polyunsaturated fatty acids such as γ-linolenic acid (GLA) and arachidonic acid similarities are presented in the cancerous breast tissue. These components act as precursors to proinflammatory eicosanoids which are tissue hormones that represent a risk factor for cancer when decomposing (99, 100). These ω-6 acids are precursors of prostaglandin E2 which have a role on angiogenesis and prevent apoptosis. Additionally, arachidonic acid has proven to be susceptible to peroxidation of lipids causing a genotoxic effect (98).

Fatty acids seem to actively participate in carcinogenesis processes in their polyunsaturated form (104, 105). Cyclooxygenase catalysis leads to prostaglandin products that

act as inflammation, anaphylactic, and vasoconstriction mediators (106). Moreover, COX-1 and -2 oxidize DGLA and EPA which are essential fatty acids, resulting in products with stronger inflammatory potential. Other examples of the lipid's role in cancer pathways are the aggressiveness of breast carcinoma, which has been suggested to have a close relation with delta-6 desaturase levels, specifically fatty acid metabolism. COX2 pathways upregulate several carcinoma pathways, its expression and activity enhanced the breast tumorigenic and metastatic potential. Therefore, fatty acid metabolism can provide an important insight in the carcinogenesis study (97).

Tumor markers are substances produced as response to cancer presence. In order to establish a marker, the peak should appear exclusively in the malignant tissue and a qualitative estimation would be recommended. The identification of biomarkers with Raman spectroscopy might help to understand the molecular mechanism behind the breast cancer disease (75). Based on the widely reported differences between normal and cancerous breast tissue fatty acids and carotenoids can play an important role as biomarkers (98).

Margins determination

The accurate identification of normal and cancerous breast tissue is of vital importance as it is a clinical tool to identify the negative safety margins of the tumor during mastectomies. Raman spectroscopy provides information regarding the nature of the tissue, and the progression states of the disease. The identification of lesions during exploratory surgeries can be achieved with Raman spectroscopy, reducing the need of re-excision procedures. Raman mapping produces images, which resemble the traditional histological images. Moreover, the implementation of probes in the "Raman biopsies" might translate into real-time, label-free and non-subjective chemical information (107). *In vivo* Raman spectra acquisition has been possible due to the use of Raman probes. The first studies evaluated its potential for intraoperative margin assessment, which was feasible in mastectomy procedures. The malignant and benign nature of the tissue was successfully identified using an established fit coefficient model. With an accuracy of 93.3% for *in vivo* measurements, this opens the possibility of spectroscopic transdermal needle measurements to be used as real time diagnosis (64, 81, 108–110).

Imaging data from Abramczyk's research group reported intense Raman peaks at around 1158 and 1518 cm^{-1}, which corresponds to carotenoids, proving that natural antioxidants are stored and reserved in adipose cells in the case of healthy tissue. A lack of intensity in these bands showed a lower contribution in the cancerous samples. The main differences between normal and cancerous tissue can be detected with the following Raman biomarkers: carotenoids, proteins, lipids and water. By paying attention to the bands associated with these biomarkers, an accurate identification of the tumor margins was achieved (64, 75, 94, 96).

Calcifications in breast lesions

Micro-calcifications have a correlation with the breast lesion state. Type 1 micro-calcification is composed of calcium oxalate and is almost exclusively present in benign cysts.

Type II is composed of calcium hydroxyapatite and its presence is often seen in proliferative lesions including hyperplastic and cancerous tissue. Therefore, the identification of both micro-calcification types is relevant for proper diagnosis. Raman spectroscopy was feasible for micro-calcification detection in fresh-excised biopsies, distinguishing between both types regardless of their size or prior radiographic identification (92, 111–113).

Furthermore, it was suggested that the use of Raman spectroscopy has a higher sensitivity to detect micro-calcifications in comparison with mammography. A series of studies on calcification detection, classification and cancer relation have demonstrated the potential of Raman spectroscopy to obtain suitable samples during biopsy procedures. Consequently, this might reduce both miss-sampling and false negatives, offering real-time feedback (111–113).

Spatially offset Raman spectroscopy (SORS) has been used to analyze and differentiate between calcifications at different depths within human and chicken breast tissue in a noninvasive protocol. The SORS technique allows a deeper analysis in comparison with conventional Raman approaches. Depths of up to 10.2 mm were tested to demonstrate the potential of this technique through different breast tissue densities. Spectral signals of the inorganic standards were achieved at 10.2 mm; however, the optimal distance was up to ~5 mm. Further studies are in progress to enhance the sensitivity of SORS at different depths. This is required considering that the flattened breast thickness is around 5 cm during mammography (114, 115).

Sample preparation and analysis procedure

Raman spectroscopy allows the analysis of samples in different states, presenting an advantage for biological research (62, 116). The technique provides the opportunity to detect considerable differences in the signal, potentially caused by the sample preparation and the nature of the tissue, i.e. cancerous, abnormal, normal. Although a number of studies have stated that more fluorescence is present in malignant than in normal tissue, but at the same time some other studies have reported that in certain types of cancers the autofluorescence is similar to that of malignant tissues (75, 78, 117). Hence, it makes it difficult to make conclusive predictions on the basis of fluorescence alone.

When fresh samples are analyzed, a higher fluorescence is expected due to the hemoglobin present in the blood, which acts as a fluorophore. Additionally, the free oxidation of the pigment component of carotenoid and lipids can contribute to the increased fluorescence on the cancerous tissue. In the literature, a discrepancy was found within the discussion of the fluorescence based on the nature of the breast tissue (80).

Several studies investigated the effect of paraffin embedding on breast tissue for Raman analysis. The dewaxing procedure has demonstrated a certain degree of fatty acids washing out from the breast tissue, which may have limited effect on the spectra from breast cancer interfering with lipids and carotenoids spectral peaks. However, the fixation and embedding of samples allows its preservation and late analysis and the method is routinely and successfully used (80, 98, 118). A number of dewaxing protocols have been specifically developed and minimum effect on the tissue is observed (116, 119).

It is important to highlight not only the relevance of the sample state, but also the protocol for spectral acquisition are important aspects to be considered. When different points are analyzed within a tumor, spectral differences are expected, as the samples can contain normal components, such as, fat and blood vessels. When mapping studies were carried out an inhomogeneous component distribution is expected. The ideal protocol for single point Raman analysis should include the spectral acquisition of several random points within the malignant tissue to avoid misleading results (80, 87, 97, 120).

Cell culture studies

Yu and coworkers focused on the identification of cell changes at the biochemical level. The use of confocal Raman microscopy provided an easy methodology to obtain sub-cellular level analysis due to its 1 μm spatial resolution. They analyzed the nucleus components in normal and transformed cells to identify the biomolecular changes caused by the tumorigenic process. Normal MCF10A and tumorigenic human breast epithelial cells (HBEC), MCF10AT, and MDA MB435 were grown in gold-coated slides and were mapped after media removal and washing. Normal HBEC nuclei were isolated then DNA, RNA and protein were extracted and placed on gold coated slides and air-dried to obtain 30 mm^2 spots. An average of 12 spectra per sample were used to establish the spectrum of proteins, RNA and DNA, and obtain the spectral fitting profiles. As expected, the MCF10AT mapping results reflected a higher content of DNA on the cell nuclei. Different protein contents were found across the cell area, where "spots" with higher content suggested the possibility of abnormal cellular activity. Nuclei study can offer a powerful tool for understanding tumorigenesis and cancer detection. As this is a genetic process, the associated changes would first occur in this part of the epithelial cell. Nuclei spectra model analysis using DNA, RNA and protein spectra fitting showed that all tumorigenic cells present a higher content of DNA material in comparison with normal HBECs. This result was associated with the aneuploidy (alterations in the chromosomes number) nature of tumorigenic cells. Tumorigenic cells showed a higher contribution of proteins; however, this was not as significant as the increase in DNA. A lack of nuclei lipid extraction protocols prevented the contribution of nuclei lipids from being evaluated in this study. When cell lines are compared, ensuring the same proliferative status is recommended, which presents a limitation. Despite this limitation, Raman spectroscopy proved its potential for quantitative analysis when methodologies such as fitting curves are used (121–123).

When immortalized and transformed cell lines were compared to normal epithelial breast cells, a higher lipid content was found in the abnormal cells. This contradicts the results of several studies where tissue was analyzed (88, 124–126). Despite the disagreement, the excess of lipid content has an important role in cell adhesion and migration. Additionally, lipid rafts oversee signaling to promote cell survival and the storage of lipids acts as a reservoir for several cell functions. Moreover, the intensity increase of phenylalanine and tryptophan can indicate the breast tissue transformation suggesting a risk of cancer development (127, 128).

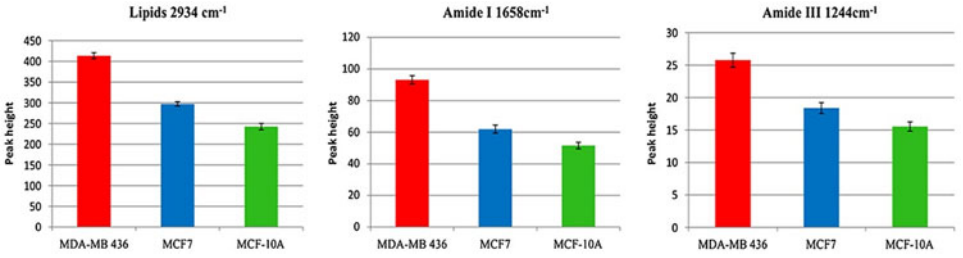

Figure 6. Peak height analysis of lipids (2934 cm^{-1}), amide I (1658 cm^{-1}) and amide III (1244 cm^{-1}) of MCF-10A, MDA-MB 436 and MCF-7 (20).

Invasive cells showed a higher lipid/carbohydrate ratio in comparison to noninvasive epithelial cells. This ratio in addition to the 1447 cm^{-1} C-H deformation band were suggested as possible markers for invasiveness based on the 100% accuracy obtained using PC-LDA analysis. Lipid rich neoplasm can reflect the increased novo lipogenesis which is associated with the accelerated membrane formation. This acceleration is caused by fast proliferation and represents a hallmark of metastatic or invasive processes (127, 129).

Two cancerous breast cell lines, MDA-MB-436 (triple negative subtype) and MCF-7 (ER + subtype), and one normal MCF-10A breast cell line were analyzed with Raman spectroscopy. Twenty spectra were collected from each cell line and multivariate analysis (PCA and LDA) was used to identify differences among the cell lines. Peaks at 2934, 1658, and 1244 cm^{-1}, associated with lipids, amide I, and III, were compared based on their intensity. The peak intensity showed differences among the cell lines as can be seen in Figure 6. As a general trend, the absolute intensity of each region decreased from MDA-MB-436 to MCF-7 to MCF-10A (20).

The score in the PCA of the lipid region, revealed that a higher content of lipids and nucleic acids were identified in the MCF-7 cell line, in comparison to the other two cell lines. However, a higher content of protein was found in the MDA-MB-436 and MCF10A cell lines. The higher content of nucleic acids might be associated with the accelerated metabolic activity or the cell density in the specific sample. The MDA-MB-436 lipid content did not seem to be considerably different from the content of lipids in the normal cell line. However, PCA identified the α-helix and β-sheet conformation of structural proteins, as a differentiator between MDA-MB-436 and MCF-10A. The chemometric model was validated using LDA, which suggested that classification was predicted with 100% sensitivity and 91% specificity (20).

Information regarding different cellular processes can be obtained by Raman analysis. Senescence or inhibition of cell division plays an important role in cancer treatment by deterring tumor growth. Raman imaging analysis demonstrated that a change on isomeric unsaturated lipid content differed between proliferating and senescent breast cancerous epithelial cells. These changes suggest an effect on the nuclear envelope composition. Stable nuclear membranes are formed by isomeric configuration, *-cis* and *-trans*, in order to monitor the transfer of macromolecules. Control proliferating cells showed both configurations, whereas senescent cells contain mainly *-cis* isomers, destabilizing the nuclear envelope, increasing the nuclear fluidity. Senescent cells spectra showed a lack of glycoprotein content on the membrane, affecting the macromolecule's

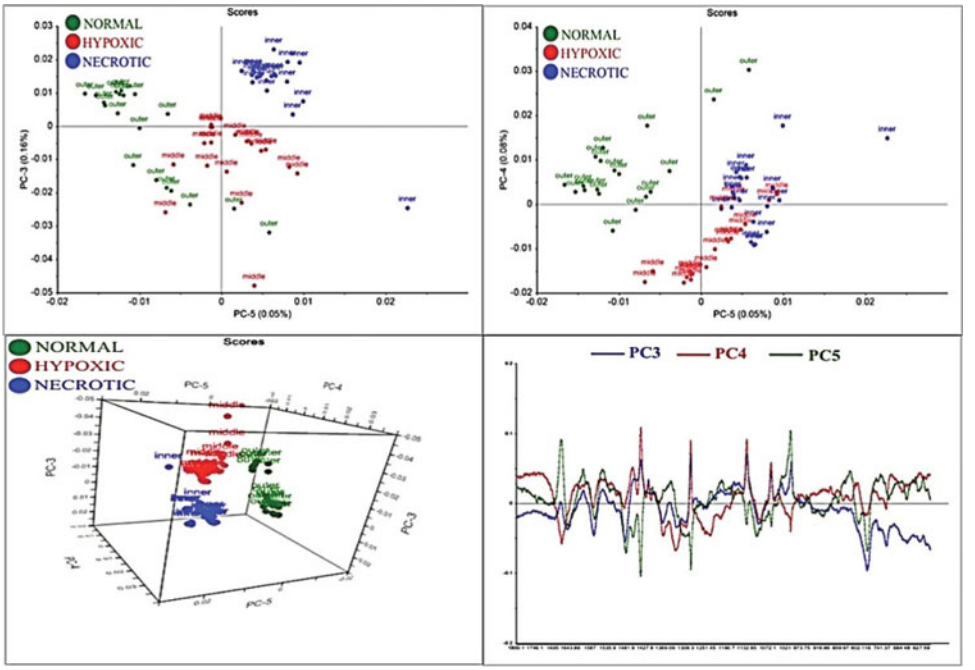

Figure 7. PCA score and loading plots of fingerprint region analysis for normal proliferating (green), hypoxic (red) and necrotic (blue) regions of T-47D spheroids based on third, fourth and fifth principal components (PC) (47).

flow through the membrane, which will disturb the proliferating cycle of the senescent cells (130).

The microenvironment of breast tumors has been widely investigated. *In vitro* models have been used to recreate the microenvironment conditions in the lab as they display anatomical characteristics of solid vascular tumor microenvironments. An example of these models are 3D cell cultures involving spheroids. The spheroids protocol involves the isolation of cells from breast sections, the growth of monolayers and their seeding in agarose. Talari et al. studied the different regions in this model using Raman spectroscopy and multivariate analysis. This model was composed by a section of a T-47D cells spheroid. Three different regions were identified through histology in the non-vascular in vitro breast cancer tumor model. The outer margin of the spheroid was characterized by a proliferative behavior which was verified with the results of the Ki67 marker analysis. The intermediate area showed a quiescent hypoxic region which was confirmed using a Hypoxyprobe kit, whilst the central region was completely necrotic. The identification of hypoxic areas is vital in tumor microenvironment research, as oxygen deprivation has been identified as a trigger for angiogenesis and therefore metastatic processes (47).

When the data obtained for the three regions were compared, differences in peak shifts and peak intensities were detected. These differences suggest that each region progressing towards necrosis faces stress. A clear classification using principal component analysis (PCA), cluster analysis (CA), and validation using linear discriminant analysis (LDA) was easily achieved. PCA was used to identify the differences in the lipids,

proteins and nucleic acids, while CA identified clusters within the high-wavenumber region, amide I and nucleic acid region (47).

PCA performed on the lipid region offered a clear separation using PC-2 and PC-4. The three regions were separated by PC-2 showing an overall higher content of lipids over proteins. However, the highest ratio was found in the proliferating region, followed by the necrotic area and the hypoxic region. The lack of oxygen supply in the hypoxic region lead to higher rates of oxidative stress, resulting in considerable lipid peroxidation processes and therefore oxidative degradation of lipids. Furthermore, PC-4 clearly separated the necrotic area spectra from the hypoxic and normal proliferative tissue. The PC-4 loading identified that a higher content of protein content was found in the necrotic area in comparison with the hypoxic area (47).

Within the results of the PC-3 and PC-4, from the fingerprint region analysis (1800–600cm^{-1}), a separation between the hypoxic area, and the normal proliferative and necrotic area was visible as presented in Figure 7. On the contrary, PC-5 presented a separation between the normal proliferative area and the necrotic area, with the hypoxic area laying in between (47).

PC-3 and PC-4 loadings reflected that a high content of lipids was found in the necrotic area in comparison with the normal proliferating area based on the 1606, 1438, and 1294 cm^{-1} vibrations. These vibrations are associated with the bending of lipids and twisting of methylene groups. The loading for PC-3 also suggested a higher content of lipidic components in the hypoxic area in comparison with the normal proliferating area. The elevated concentration of proteins and nucleic acids in the hypoxic area suggests that both biomolecules will assist the stressed oxygen deprived cells to face necrosis through genetic metabolic pathways. Moreover, the loading of PC-3 indicated a lower protein content in the necrotic area in comparison to the normal proliferative area. This finding was supported by the protein vibrational modes found at 1668, 1237, and 1004 cm^{-1} which are associated with C=O of amide I, amide III and phenylalanine. Low contents of nucleic acids were detected in the necrotic area based on the peaks at 1374, 1340, and 782. These peaks are associated with adenine, thymine and guanine bases of DNA, nucleic acid modes, and DNA assignments. The PC-5 loading confirmed the previous findings by revealing a high protein and nucleic acid content in the normal proliferating area using the 756 cm^{-1} (tryptophan) and 832 cm^{-1} (O–P–O stretches of nucleotides) Raman shifts (47).

When the amide region (1800–1510 cm^{-1}) was analyzed with PCA, all areas of the spheroid section were separated by PC-3 and PC-4. This separation revealed that a low amide I content is present in the necrotic and hypoxic areas based on the anti-parallel β-sheets of amide I at 1670 cm^{-1}. Changes in amide I suggest modifications in the ECM which is mainly formed by collagen. The ECM plays a vital role in tumor progression and metastasis. It has been reported that hypoxia processes have a direct effect on the collagen production and remodeling through their involvement in the transcriptional status of procollagen genes. Furthermore, the loading of PC-3 reflected a high content of tryptophan in the normal proliferating area. PC-5 showed a separation between the necrotic area, and the normal proliferating and hypoxic area. The clear clustering of the hypoxic area spectra indicates differences in the amide I composition, confirming an accelerated protein metabolism associated with ECM changes (47).

In the high-wavenumber range, cluster analysis showed more similarities between the necrotic and normal proliferating areas, than the hypoxic area. However, when the amide I and nucleic acid regions were analyzed, the normal proliferative and hypoxic area showed more similarities than the necrotic area (47).

Metastasis and invasive processes

Tracking the biochemical changes associated with metastatic lesions can offer a clearer understanding of the tissue-specific adaptations to invasive metastatic processes. The importance of studying metastatic or secondary tumors resides in the variability between the first lesion and the spread. The primary and secondary tumor might express different biomarkers and hormones receptors and can be targeted with different therapies. The study of the metastatic processes is relevant as there are different features in each step that are not well-understood. These features include the capacity of cells to survive and populate in other non-related tissues under harsh conditions (131).

Analyzing metastatic tissue offers insight into the biological changes at the molecular level associated with the invasive lesion. Mice isogenic metastatic lesions, primary tumor and the metastatic breast cancer cells were grown. Cells isolated from the primary breast tumor and metastatic lesions in lung, brain, liver, and spine were analyzed. These sites were chosen as they are the most common tissues affected by breast cancer metastasis. PCA and a spectral-derived dendrogram showed spectral differences proposing different molecular alterations and molecular adaptations in the different tissues analyzed. The previous statement strongly suggests site-specific adaptations associated with metastatic processes. However, certain similarities were found between liver and brain metastases, and were confirmed by metabolomics. Based on the model constructed by this study a 96.8% classification accuracy was achieved. The PC spectra obtained showed that the following regions were responsibly of the classification of the cell lines: 1000–1006 cm^{-1}, 1136–1211 cm^{-1}, 1298–1330 cm^{-1}, and 1435–1470 cm^{-1}. Lipids, proteins, and nucleic acids were identified as responsible for the variation among cells. Supported by metabolomics the differences were attributed to the metabolism, microenvironment, functions requirements, and development of the cell lines. In this study, motility assays were performed but were inconclusive. However, cancerous cells showed high adaptability to low nutrient conditions under the test conditions serving as a proof of its adaptation to hostile microenvironments (131).

The metastasis effect caused by breast cancer was studied in the aorta of murine models using mapping analysis. After metastasis was induced by implantation of 4T1 tumor cells, the aorta was analyzed at different depths. Different contents of lipids and proteins were found among the metastatic and control endothelium layer of the mice vascular walls. The control endothelium layers presented a higher content of lipids and lower protein content than other vascular wall layers. Metastatic samples, however, showed a similar lipid/protein ratio among all layers. Metastatic processes alter the biomolecule composition and content of endothelial tissue by decreasing the lipid content (to 4–7%) and the overproduction of proteins (12–18% by volume) similar to what has been reported in breast cancer tissue. It was identified that these changes were limited to the endothelial layer. Lipid drops can be associated with cellular endothelial injury

while the protein overexpression is suggested due to pro-inflammatory and pro-thrombotic endothelial phenotype (132). Elevated protein content can also reflect cell division activity and proliferation in addition to migration which are characteristic of the carcinogenesis process (98).

An insight into breast cancer cells transitioning from epithelial to mesenchymal tissue was obtained with Raman spectroscopy. The analysis confirmed changes in metabolic features proving with 94% sensitivity and 100% of specificity that highly metastatic cells increase the tryptophan levels but maintain low fatty acids content (70).

The biochemical premetastatic effect of breast cancer cell lines in lungs demonstrated that the ECM changes prior to the invasion of cancer cells into other organs. These changes were associated with collagen and proteoglycan components that prepare the premetastatic niche (133).

Raman sensitivity for chemical analysis has allowed the detection of changes on the extracellular matrix. These changes are usually associated with variations in the content of collagen, elastin, and proteoglycan. These affectations have a stretch association with stromal desmoplasia, which is a malignancy response. Another possible malignancy indicator is the presence of increased vasculature that chemically will be identified by an increase in hemoglobin (72, 134).

Raman spectroscopy does not only characterize the chemical composition, but it also provides an overview of the structural characteristics of those molecules (131). These structural changes can be used as indicative of collagen affectations which can be reflected in scarring, contraction, and neoplasm growth.

Epigenetic and gene alterations

Epigenetic alterations had been suggested as the cause of certain types of cancer (135). Some of these alterations include the methylation of DNA and histone. These alterations affect the transcription and therefore the post translational modifications by varying the acetylation, phosphorylation, and methylation. Raman spectroscopy demonstrated potential to track acetylation and methylation processes serving as an epigenetic modification monitoring test. The monitoring was achieved by focusing on lysine, which is highly affected by epigenetic modifications and is involved in post-translational regulatory mechanisms of protein activity. Additionally, the acetylation and methylation of lysine affects the cell cycle, actin nucleation and other cellular processes (135). PCA revealed that 91.3% specificity and 85.3% sensitivity was achieved on this study when monitoring the acetyl group observed at 2927–2942 cm^{-1} and the methyl group at 2970 cm^{-1} of breast cancer samples. The spectral profiles suggested that the Raman shift from 2905 to around 2942 cm^{-1} from normal to cancerous tissue can be used to define the aggressiveness of the disease.

The effect of relevant genes in metastasis suppression has been explored with Raman spectroscopy. Wu et al. analyzed Breast Cancer Metastasis Suppressor 1gene (BRMS1) and its effect on MDA-MB-435 human breast carcinoma cells with Raman and atomic force microscopy (AFM). The expression of BRMS1 is shown to induce alteration on MDA-MB-435 human breast carcinoma cells phenotype resulting in changes in cell adhesion, structure rearrangement and decrease of epidermal growth factor receptor

(EGFR) expression. The Raman spectra collected on this study revealed a decrease on the intensity in the general 453/BRMS1 spectrum. The intensity reduction suggested a decrease of the biochemical components of the cancerous cell in comparison with the 435 alone. Although an overall similarity in band assignments was found in this work, the results suggest a slight alteration in the content of biochemical components and not exclusively a change in the composition of the cell surface as a response of the BRMS1 suppressor gene expression. AFM confirms changes in the biomechanical properties in 435/BRMS1 cells attributing the metastatic nature of the 435 cells to them (136).

Raman imaging

Raman imaging (RI) allows optical and spectral sectioning in three dimensions. RI has several advantages such as providing biochemical information without contrast agents. This is achieved using the natural contrast offered by soft tissues. Raman probes can be integrated into clinical use allowing Raman imaging to be used *in vivo*. Contrast-enhancing probes can detect specific DNA sequences, gene products and intracellular processes. Moreover, RI can allow studying structures and pathologies located in orientation sensitive tissues with a high resolution. Real-time diagnosis is a possibility offered by the incorporation of catheter-based micro-transducers when using RI *in vivo*. Due to these advantages, RI has been considered a competitive technique against other confocal fluorescence microscopies (64).

Raman imaging of breast samples was obtained with good contrast, which was attributed to the carotenoids, fatty acids and proteins in the sample. Breast cancer Raman imaging results confirmed a greater contribution of protein, whereas normal breast tissue indicated the existence of different lipids with a high content of oleic acid derivatives. Surmacki et al. identified differences in the water content, when working with fresh and frozen samples. Cancerous samples presented more water than normal tissue, likely due to the high content of hydrophobic lipid components in non-cancerous tissue. This difference was identified by the intensity variation in the OH stretching band at higher wavenumbers. Water variations have not been reported by other authors that worked with processed samples, as this process involves dehydration (89).

Nodal evaluation is an important feature to assess in breast cancer, as they represent one of the first routes for metastatic processes (137). Nodal sections were tested using Raman mapping analysis in which different biomolecules' contributions were detected among metastatic lesions. These results indicate the technique's potential not only to assess breast and nodal tissue but also to offer a complete analysis of the biochemical changes in different tissues associated with metastasis (138).

The understanding of cell cycles and cell growth can help to develop efficient therapies, as most of the chemotherapy drugs target the cell cycle (139, 140). Cell behavior and native properties of mammalian cells have been studied with Raman spectroscopy, suggesting that some biochemical changes might be associated with the proliferation state of the disease. Proliferation studies of rat mammalian cells using a Raman probe system showed a higher content of nucleic acid and protein material in proliferating cells, in comparison with plateau cells. Plateau cells were in their majority (80%) in the G1/G0 phase and $<50\%$ exponential cells were in the G1 phase of the cell cycle.

Proliferative state can be monitored taking into consideration cell cycle distributions, cell density and cell volume (larger size just before mitosis, in G2 phase) (141).

Analysis of serum has demonstrated potential for breast cancer diagnosis. Serum from 11 patients diagnosed with breast cancer were analyzed and compared with serum from healthy patients. This analysis produced results with similar spectra, with differences in intensity and shifts in some bands. These bands included proteins, phospholipids, polysaccharides, and beta-carotene. Although PCA only offered a clear separation for the samples of metastatic patients and did not offer a clear separation between the control and the cancerous samples, LDA was able to discriminate between both groups with 92.2% sensitivity and 78% specificity (142).

Bitar Carter et al. analyzed 51 different areas of defrosted normal breast tissue and malignant and benign neoplasm with FT-Raman spectroscopy. Similarities to the breast tissue layout spectra were easily detected, however band shifts were present in the data. The main differences were found in the amide region. The irregular surface of the tissue potentially caused poor scattering, resulting in a lower intensity in the spectrum of diseased tissue (143).

Surface enhanced Raman spectroscopy (SERS) studies

Raman scattering is considered weak in comparison with the signals of other techniques. This problem can be reduced using structured metal surfaces, which enhances the scattering efficiency. Taking advantage of the surface plasmon resonance in the metallic surface or nanoparticles can lead to an increase in the detected Raman signal by up to 11 orders. This amplification approach is known as surface-enhanced Raman spectroscopy (SERS). Oncogene biomolecules are produced in small quantities around the micro to picomolar concentrations when the disease presents. Therefore, sensitive and highly chemical specific techniques are needed to detect oncogenes. Owing to the high sensitivity required, different amplification approaches integrated to Raman spectroscopy and probes had been tested. These approaches include the incorporation of nanoparticles into the probes. Furthermore, the incorporation of labeling techniques such as antibody-antigen pairing, complexation, DNA hybridization and aptamer recognition which is a sequence of a single nucleic acid strand, to achieve a targeted specificity has also attracted a lot of attention (64).

Nanoparticle SERS probes have been used to target relevant components in breast tumors demonstrating their potential as cytodiagnostic systems. For example, functionalized gold nanoparticles were used as probes for hypersialylation differentiation in different tumors. Hypersialylation is represented by increased levels of sialic acid. Sialic acid expression on the tumor surface is closely related to the tumor metastatic potential. Therefore, SERS can facilitate the tissue characterization and its evaluation before and after therapy, and during drug testing (144).

Different research groups using SERS to target HER2 on breast cancer cells have used the combination of nanoparticles and antibody-antigen pairing. The targeting and quantification of the overexpression of HER2 receptor is highly relevant due to the 20% detection inaccuracy and time-consuming process followed nowadays. The identification of the HER2 status was achieved with 100% sensitivity and 99% specificity using SERS.

Similar methodologies have been used to identify and, in some cases, quantification of PSA, BRCA1, EGFR, CD44, GA733-2, MUC1, and TGFβRII in cancerous cells. A Raman active label, usually nanoparticles or quantum dots; a probe molecule that specifically targets interest species (e.g. antibody-antigen) and a protective layer such as silica capsules form all these systems (64, 145–158).

Serum research has been conducted in which gold nanoparticles were added as signal enhancers for SERS analysis. The main differences between the breast cancer and control spectra were the content of glutathione, tryptophan, β carotene, and amide III resulting in a model with 96% sensitivity and 87% specificity (159).

The use of different drugs and chemicals with the purpose of improving imaging can be tracked in the breast tissue using SERS and other complementary techniques. For example, aluminum phtalocyanine, a photosensitive chemical used in photodynamic diagnosis (PDD), photoimmunotherapy (PIT), and photodynamic therapy was detected with Raman spectroscopy in normal and cancerous breast tissue (160).

Current challenges of Raman spectroscopy for breast analysis

Bioanalytical measurements using Raman spectroscopy present some limitations, such as traceable quantification. When analytes with weak signals are the target of the analysis, techniques with higher sensitivities such as SERS are required. Sample preparation also plays an important role. Due to the integration of confocal and probe systems, the topography and dispersion of the sample might affect the quantification and comparison of cases. When turbid samples are analyzed and nonspecific areas are selected, robust calibration models are needed to ensure reliable and quantitative measurements (161). In addition, there are challenges in the use of probes and *in vivo* analysis. Background fluorescence and artifacts need to be overcome before introducing Raman spectroscopy as a diagnostic tool. Constructing robust chemometric models is required for automation and objective diagnosis (162).

These limitations have become less significant with technological advances. Optical filters and photon detectors have improved sensitivity. Using a larger range of excitation, sources reduces fluorescence. The ability to construct predicting models has improve with user-friendly software packages and increased computational power (163).

Clinical relevance and future directions

Raman spectroscopy has been demonstrated as a feasible clinical diagnostic tool for breast cancer. Additionally, understanding invasive processes has been enriched using RS. The chemical information obtained with this technique allows quantitative and qualitative analysis. The works revised in this article support future clinical implementations of this technique. It is clear that more work is required to improve the technology and facilitate its clinical use and data processing. To accomplish this, multidisciplinary collaboration between researchers, companies, and clinicians is indispensable.

Standardization of spectral data is another important facet which requires establishing. It will be useful for researchers across the globe to collaborate and demonstrate reproducibility, sensitivity and specificity of the spectral data. This will help in

increasing confidence among the clinicians and rapidly bring this technique to the armory of surgeons, oncologists, and pathologists.

Raman spectroscopy has the potential to offer a real-time analysis/diagnosis *in vivo* with excellent accuracy and is capable of maintaining this accuracy in *ex vivo* analysis after several years. Furthermore, Raman spectroscopy can provide practitioners and researchers with chemical information reflecting changes at tissue level. In clinical practice, these changes influence the treatment strategies. In practical research, these insights help to understand carcinogenesis and invasive progressions, accelerating the development of new treatments.

Summary

Raman spectroscopy has become a formidable technique for breast tissue analysis. It can be used *ex vivo*, *in vitro* and *in vivo* with excellent results containing important biochemical information. This work contributes to the field by summarizing key findings in breast spectroscopic studies and offering significant assignments and frequencies characteristic of breast.

Due to its chemical specificity, Raman spectroscopy has been used in oncology research to identify biomarkers for breast cancer and other breast pathologies. Owing to the nature of the technique, Raman spectroscopy has the potential of immediate breast analysis and therefore diagnosis when integrated into biopsy procedures.

Identification of breast cancer, and classification has been achieved with Raman spectroscopy among malignant, benign, and normal tissue. Correlating the chemical composition to breast cancer grade has been assessed and biomarkers such as carotenoids have been identified. Cell studies on cancerous and epithelial mammary cells have been revised identifying changes associated with proliferation and lipid oxidation which might contribute to the invasive process. Several advances have been recognized in the literature and the use of more sophisticated systems, such as SERS, allowed the identification and quantification of relevant substances, proteins and genes associated with breast cancer such as HER2, PSA, BRCA1, EGFR, CD44, GA733-2, MUC1, and TGFβRII.

Future prospects in terms of clinical applications include the integration of Raman spectroscopy into real-time diagnostic tests, and margin assessment during mastectomies. Raman spectroscopy has the potential for functional imaging, once the limitations of existing probes are overcome. Raman spectroscopy integrated with a fiber optic probe can be used to generate chemical images of the tissue. In addition, the combination of Raman spectroscopy with existing imaging techniques can complement breast tissue assessment. RS can be used as a characterization and tracking technique during clinical trials, assessing the effect of new drugs and cancer progression.

Several improvements have evolved the technology and data modeling techniques for tissue analysis in the past years. These enhancements give the scope to bringing the pathology and chemical characterization approaches to the operating table. Rapid and reliable tissue assessment, prompt treatment delivery, and the reduction of secondary procedures add an important value to pathology, oncology medicine, and patient care.

This review listed and revised substantial accomplishments in the latest breast cancer research with Raman spectroscopy. The current data highlights the importance of RS and its remarkable clinical potential. These findings contribute in several ways to our understanding of breast cancer and provide a basis for analysis with Raman spectroscopy.

References

1. The Global Cancer Observatory. (2018) Breast Cancer Fact sheet: Globocan 2018. http://gco.iarc.fr/today/data/factsheets/cancers/20-Breast-fact-sheet.pdf (Accessed September 2018).
2. Ferlay, J., Soerjomataram, I., Dikshit, R., Eser, S., Mathers, C., Rebelo, M., Parkin, D., Forman, D., and Bray, F. (2015) Cancer incidence and mortality worldwide: Sources, methods and major patterns in GLOBOCAN 2012. *Int. J. Cancer* 136 (5): 359–386.
3. Titloye, N. A., Foster, A., Omoniyi-Esan, G. O., Komolafe, A. O., Daramola, A. O., Adeoye, O. A., Adisa, A.O., Manoharan, A., Pathak, D., D"Cruz, M.N., Alizadeh, Y., and Lewis, P.D. (2016) Histological features and tissue microarray taxonomy of Nigerian breast cancer reveal predominance of the high-grade triple-negative phenotype. *Pathobiology* 83 (1): 24–32.
4. Kamangar, F., Dores, G. M., and Anderson, W. F. (2006) Patterns of cancer incidence, mortality, and prevalence across five continents: Defining priorities to reduce cancer disparities in different geographic regions of the world. *J. Clin. Oncol.* 24 (14): 2137–2150.
5. McPherson, K., Steel, C. M., and Dixon, J. M. (2009) 5 Breast cancer—epidemiology, risk factors, and genetics. *ABC Breast Dis.* 69: 24.
6. Torre, L. A., Siegel, R. L., Ward, E. M., and Jemal, A. (2016) Global cancer incidence and mortality rates and trends-an update. *Cancer Epidemiol. Biomarkers Prev.* 25 (1): 16–27.
7. World Health Organization. (2016) Global Health Estimates 2015: deaths by cause, age, sex, by country and by region, 2000-2015. WHO, Geneva.
8. Vendrell, M., Maiti, K. K., Dhaliwal, K., and Chang, Y.-T. (2013) Surface-enhanced Raman scattering in cancer detection and imaging. *Trends Biotechnol.* 31 (4): 249–257.
9. Asiago, V. M., Alvarado, L. Z., Shanaiah, N., Gowda, G. A. N., Owusu-Sarfo, K., Ballas, R. A., and Raftery, D. (2010) Early detection of recurrent breast cancer using metabolite profiling. *Cancer Res.* 70 (21): 8309–8318.
10. Schreer, I., and Lüttges, J. (2005) Breast cancer: Early detection. In *Radiologic-pathologic correlations from head to toe*, Gourtsoyiannis, N.C., Ros, P.R., Eds. Springer, Berlin, Heidelberg, pp. 767–784.
11. UK Trial of Early Detection of Breast Cancer Group. (1988) First results on mortality reduction in the UK trial of early detection of breast cancer. *Lancet* 332 (8608): 411–416.
12. Ma, X.-J., Salunga, R., Tuggle, J. T., Gaudet, J., Enright, E., McQuary, P., … Zhang, B. M. (2003) Gene expression profiles of human breast cancer progression. *Proc. Natl. Acad. Sci. U.S.A.* 100 (10): 5974–5979.
13. May, C. D., Sphyris, N., Evans, K. W., Werden, S. J., Guo, W., and Mani, S. A. (2011) Epithelial-mesenchymal transition and cancer stem cells: A dangerously dynamic duo in breast cancer progression. *Breast Cancer Res.* 13 (1): 202.
14. Weigelt, B., Peterse, J. L., and Van't Veer, L. J. (2005) Breast cancer metastasis: Markers and models. *Nat. Rev. Cancer* 5 (8): 591–602.
15. Kendall, C., Isabelle, M., Bazant-Hegemark, F., Hutchings, J., Orr, L., Babrah, J., … Stone, N. (2009) Vibrational spectroscopy: A clinical tool for cancer diagnostics. *Analyst* 134 (6): 1029–1045.
16. Talari, A. C. S., Movasaghi, Z., Rehman, S., and Rehman, I. U. (2015) Raman spectroscopy of biological tissues. *Appl. Spectrosc. Rev.* 50 (1): 46–111.

17. Jermyn, M., Desroches, J., Aubertin, K., St-Arnaud, K., Madore, W.-J., De Montigny, E., … Petrecca, K. (2016) A review of Raman spectroscopy advances with an emphasis on clinical translation challenges in oncology. *Phys. Med. Biol.* 61 (23): R370.
18. Santos, I. P., Barroso, E. M., Schut, T. C. B., Caspers, P. J., van Lanschot, C. G. F., Choi, D.-H., … Verdijk, R. M. (2017) Raman spectroscopy for cancer detection and cancer surgery guidance: Translation to the clinics. *Analyst* 142 (17): 3025–3047.
19. Rehman, I. ur. (2013) *Vibrational spectroscopy for tissue analysis*. CRC Press, Boca Raton.
20. Talari, A. C. S., Evans, C. A., Holen, I., Coleman, R. E., and Rehman, I. U. (2015) Raman spectroscopic analysis differentiates between breast cancer cell lines. *J. Raman Spectrosc.* 46 (5): 421–427.
21. Austin, L. A., Osseiran, S., and Evans, C. L. (2016) Raman technologies in cancer diagnostics. *Analyst* 141 (2): 476–503.
22. Dabbs, D. J. (2012) *Breast pathology*. Elsevier Health Sciences. Philadelphia, USA.
23. Polyak, K. (2011). Heterogeneity in breast cancer.*The Journal of clinical investigation*, *121*(10), 3786–3788.
24. Hanahan, D., and Weinberg, R. A. (2000) The hallmarks of cancer. *Cell* 100 (1): 57–70.
25. Ellis, I., Al-Sam, S., Anderson, N., Carder, P., Deb, R., Girling, A., … Lee, A. H. S. (2016) Pathology reporting of breast disease in surgical excision specimens incorporating the dataset for histological reporting of breast cancer. The Royal Collage of Pathologists, London.
26. Alizart, M., Saunus, J., Cummings, M., and Lakhani, S. R. (2012) Molecular classification of breast carcinoma. *Diagn. Histopathol.* 18 (3): 97–103.
27. Ravert, P. K., and Huffaker, C. (2010) Breast cancer screening in women: An integrative literature review. *J. Am. Acad. Nurse Pract.* 22 (12): 668–673.
28. Thiery, J. P. (2002) Epithelial- mesenchymal transitions in tumour progression. *Nat. Rev. Cancer* 2 (6): 442.
29. Knowles, M. A. (2005) *Introduction to the cellular and molecular biology of cancer* (4th ed.). Oxford University Press, New York.
30. Pusztai, L., Mazouni, C., Anderson, K., Wu, Y., and Symmans, W. F. (2006) Molecular classification of breast cancer: Limitations and potential. *Oncologist* 11 (8): 868–877.
31. Guedj, M., Marisa, L., De Reynies, A., Orsetti, B., Schiappa, R., Bibeau, F., … Longy, M. (2012) A refined molecular taxonomy of breast cancer. *Oncogene* 31 (9): 1196–1206.
32. Callagy, G., Cattaneo, E., Daigo, Y., Happerfield, L., Bobrow, L. G., Pharoah, P. D. P., and Caldas, C. (2003) Molecular classification of breast carcinomas using tissue microarrays. *Diagn. Mol. Pathol.* 12 (1): 27–34.
33. Wold, S. (1991) Chemometrics, why, what and where to next? *J. Pharm. Biomed. Anal.* 9 (8): 589–596.
34. Hopke, P. K. (2003) The evolution of chemometrics. *Anal. Chim. Acta* 500 (1): 365–377.
35. Miller, J. N. (2005) *Statistics and chemometrics for analytical chemistry [electronic resource]* (5th ed.). Pearson/Prentice Hall, Harlow, England; New York.
36. Geladi, P. (2003) Chemometrics in spectroscopy. Part 1. Classical chemometrics. *Spectrochim. Acta Part B-At. Spectrosc.* 58 (5): 767–782.
37. Izenman, A. J. (2013) Linear discriminant analysis. In *Modern multivariate statistical techniques*, Izenman, A.J., Eds. Springer, New York, NY, pp. 237–280.
38. Wang, S., Lu, J. F., Gu, X. J., Du, H. S., and Yang, J. Y. (2016) Semi-supervised linear discriminant analysis for dimension reduction and classification. *Pattern Recognit.* 57: 179–189.
39. Chan, H. P., Wei, D. T., Helvie, M. A., Sahiner, B., Adler, D. D., Goodsitt, M. M., and Petrick, N. (1995) Computer-aided classification of mammographic masses and normal tissue - linear discriminant-analysis in texture feature space. *Phys. Med. Biol.* 40 (5): 857–876.
40. Guo, Y. Q., Hastie, T., and Tibshirani, R. (2007) Regularized linear discriminant analysis and its application in microarrays. *Biostatistics* 8 (1): 86–100.

41. Nazeer, S. S., Saraswathy, A., Gupta, A. K., and Jayasree, R. S. (2014) Fluorescence spectroscopy to discriminate neoplastic human brain lesions: A study using the spectral intensity ratio and multivariate linear discriminant analysis. *Laser Phys.* 24 (2):025602.
42. Ding, H., Cao, M., DuPont, A. W., Scott, L. D., Guha, S., Singhal, S., Younes, M., Pence, I., Herline, A., Schwartz, D., Xu, H (2016) Discrimination of inflammatory bowel disease using Raman spectroscopy and linear discriminant analysis methods. Proceedings of Biomedical Vibrational Spectroscopy 2016: Advances in Research and Industry, San Francisco, California, United States, February 13-14.
43. Felten, J., Hall, H., Jaumot, J., Tauler, R., De Juan, A., and Gorzsás, A. (2015) Vibrational spectroscopic image analysis of biological material using multivariate curve resolution–alternating least squares (MCR-ALS). *Nat. Protoc.* 10 (2): 217.
44. Narice, B. F., Martínez, M. A. G., Amabebe, E., Pacheco, D. L., Rehman, I. U., and Anumba, D. O. (2018) Spectroscopic techniques as potential screening tools for preterm birth: A review and an exploratory study. *Appl. Spectrosc. Rev.* 1–20. doi: 10.1080/05704928.2018.1473873
45. Yamaguchi, S., Fukushi, Y., Kubota, O., Itsuji, T., Ouchi, T., and Yamamoto, S. (2016) Brain tumor imaging of rat fresh tissue using terahertz spectroscopy. *Sci. Rep.* 6: 30124.
46. DePaoli, D., Lapointe, N., Messaddeq, Y., Parent, M., and Côté, D. (2018) Intact primate brain tissue identification using a completely fibered coherent Raman spectroscopy system. *Neurophotonics*, *5*(3), 035005.
47. Talari, A. C. S., Raza, A., Rehman, S., and Rehman, I. U. (2017) Analyzing normal proliferating, hypoxic and necrotic regions of T-47D human breast cancer spheroids using Raman spectroscopy. *Appl. Spectrosc. Rev.* 52 (10): 909–924.
48. Frost, J., Ludeman, L., Hillaby, K., Gornall, R., Lloyd, G., Kendall, C., … Stone, N. (2017) Raman spectroscopy and multivariate analysis for the non invasive diagnosis of clinically inconclusive vulval lichen sclerosus. *Analyst* 142 (8): 1200–1206.
49. Cals, F. L. J., Koljenović, S., Hardillo, J. A., de Jong, R. J. B., Schut, T. C. B., and Puppels, G. J. (2016) Development and validation of Raman spectroscopic classification models to discriminate tongue squamous cell carcinoma from non-tumorous tissue. *Oral Oncol.* 60: 41–47.
50. Morgan, M. S. C., Lay, A. H., Wang, X., Kapur, P., Ozayar, A., Sayah, M., … Cadeddu, J. A. (2016) Light reflectance spectroscopy to detect positive surgical margins on prostate cancer specimens. *J. Urol.* 195 (2): 479–484.
51. Theophilou, G., Lima, K. M. G., Martin-Hirsch, P. L., Stringfellow, H. F., and Martin, F. L. (2016) ATR-FTIR spectroscopy coupled with chemometric analysis discriminates normal, borderline and malignant ovarian tissue: Classifying subtypes of human cancer. *Analyst* 141 (2): 585–594.
52. Dieing, T., Hollricher, O., and Toporski, J. (2011) *Confocal Raman microscopy*. Springer, c2011, Heidelberg; London.
53. Symmans, W. F., Wei, C., Gould, R., Yu, X., Zhang, Y., Liu, M., … Sinn, B. (2017) Long-term prognostic risk after neoadjuvant chemotherapy associated with residual cancer burden and breast cancer subtype. *J. Clin. Oncol.* 35 (10): 1049–1060.
54. Conti, C. J. (2010). Mechanisms of Tumor Progression. In *Comprehensive Toxicology*, McQueen, C., Eds. Elsevier: Smithville, TX, pp. 335–347
55. Cortez, M. A., Ivan, C., Zhou, P., Wu, X., Ivan, M., and Calin, G. A. (2010) microRNAs in cancer: From bench to bedside. In *Advances in cancer research*, George, F., Woude, V., Klein, G., Eds. Elsevier, USA, Vol. 108, pp. 113–157.
56. Brettingham-Moore, K. H., and Taberlay, P. C. (2016) Cancer epigenetics. In *Drug discovery in cancer epigenetics*, Egger, G., Arimondo, P., Eds. Elsevier, Australia, pp. 41–59.
57. Huang, R. Y., and Reardon, D. A. (2017) Imaging studies in immunotherapy. In *Translational immunotherapy of brain tumors*, Sampson, J., Eds. Elsevier, Boston, MA, pp. 149–179.
58. Korkaya, H., Davis, A., and Wicha, M. S. (2015) Cancer stem cells and the microenvironment. *Mol. Basis Cancer* 10: 157–164.e3.

59. Yokota, J. (2000) Tumor progression and metastasis. *Carcinogenesis* 21 (3): 497–503.
60. Schmadeka, R., Harmon, B. E., and Singh, M. (2014) Triple- negative breast carcinoma: Current and emerging concepts. *Am. J. Clin. Pathol.* 141 (4): 462.
61. Minn, A. J., Gupta, G. P., Siegel, P. M., Bos, P. D., Shu, W., Giri, D. D., … Massagué, J. (2005) Genes that mediate breast cancer metastasis to lung. *Nature* 436 (7050): 518.
62. Kong, K., Kendall, C., Stone, N., and Notingher, I. (2015) Raman spectroscopy for medical diagnostics—From in-vitro biofluid assays to in-vivo cancer detection. *Adv. Drug Deliv. Rev.* 89: 121–134.
63. Cheng, J.-X., Jia, Y. K., Zheng, G., and Xie, X. S. (2002) Laser-scanning coherent anti-stokes Raman scattering microscopy and applications to cell biology. *Biophys. J.* 83 (1): 502–509.
64. Abramczyk, H., and Brozek-Pluska, B. (2013) Raman imaging in biochemical and biomedical applications. Diagnosis and treatment of breast cancer. *Chem. Rev.* 113 (8): 5766–5781.
65. Schaeberle, M. D., Kalasinsky, V. F., Luke, J. L., Lewis, E. N., Levin, I. W., and Treado, P. J. (1996) Raman chemical imaging: Histopathology of inclusions in human breast tissue. *Anal. Chem.* 68 (11): 1829–1833.
66. Orringer, D. A., Pandian, B., Niknafs, Y. S., Hollon, T. C., Boyle, J., Lewis, S., … Maher, C. O. (2017) Rapid intraoperative histology of unprocessed surgical specimens via fibre-laser-based stimulated Raman scattering microscopy. *Nat. Biomed. Eng.* 1: 27.
67. Figueiredo, C. A., and Rutka, J. T. (2017) Diagnostic imaging: Intraoperative virtual histology. *Nat. Biomed. Eng.* 1: 33.
68. Manoharan, R., Wang, Y., and Feld, M. S. (1996) Histochemical analysis of biological tissues using Raman spectroscopy. *Spectrochim. Acta Part A Mol. Biomol. Spectrosc.* 52 (2): 215–249.
69. Frank, C. J., Redd, D. C. B., Gansler, T. S., and McCreery, R. L. (1994) Characterization of human breast biopsy specimens with near-IR Raman spectroscopy. *Anal. Chem.* 66 (3): 319–326.
70. Marro, M., Nieva, C., Sanz-Pamplona, R., and Sierra, A. (2014) Molecular monitoring of epithelial-to-mesenchymal transition in breast cancer cells by means of Raman spectroscopy. *Biochim. Biophys. Acta - Mol. Cell Res.* 1843 (9): 1785–1795.
71. Allred, D. C., Clark, G. M., Elledge, R., Fuqua, S. A. W., Brown, R. W., Chamness, G. C., … McGuire, W. L. (1993) Association of p53 protein expression with tumor cell proliferation rate and clinical outcome in node-negative breast cancer. *JNCI J. Natl. Cancer Inst.* 85 (3): 200–206.
72. Manoharan, R., Shafer, K., Perelman, L., Wu, J., Chen, K., Deinum, G., … Dasarl, R. R. (1998) Raman spectroscopy and fluorescence photon migration for breast cancer diagnosis and imaging. *Photochem. Photobiol.* 67 (1): 15–22.
73. Monaco, M. E. (2017) Fatty acid metabolism in breast cancer subtypes. *Oncotarget* 8 (17): 29487.
74. Kinlaw, W. B., Baures, P. W., Lupien, L. E., Davis, W. L., and Kuemmerle, N. B. (2016) Fatty acids and breast cancer: Make them on site or have them delivered. *J. Cell. Physiol.* 231 (10): 2128–2141.
75. Brożek-Płuska, B., Placek, I., Kurczewski, K., Morawiec, Z., Tazbir, M., and Abramczyk, H. (2008) Breast cancer diagnostics by Raman spectroscopy. *J. Mol. Liq.* 141 (3): 145–148.
76. Ames, B. N. (1989) Endogenous DNA damage as related to cancer and aging. *Mutat. Res. Mol. Mech. Mutagen.* 214 (1): 41–46.
77. Hoeijmakers, J. H. J. (2009) DNA damage, aging, and cancer. *N. Engl. J. Med.* 361 (15): 1475–1485.
78. Haka, A. S., Shafer-Peltier, K. E., Fitzmaurice, M., Crowe, J., Dasari, R. R., Feld, M. S., and Verma, I. M. (2005) Diagnosing breast cancer by using Raman spectroscopy. *Proc. Natl. Acad. Sci. U.S.A.* 102 (35): 12371–12376.

79. Shafer-Peltier, K. E., Haka, A. S., Fitzmaurice, M., Crowe, J., Myles, J., Dasari, R. R., and Feld, M. S. (2002) Raman microspectroscopic model of human breast tissue: Implications for breast cancer diagnosis in vivo. *J. Raman Spectrosc*. 33 (7): 552–563.
80. Rehman, S., Movasaghi, Z., Tucker, A. T., Joel, S. P., Darr, J. A., Ruban, A. V, and Rehman, I. U. (2007) Raman spectroscopic analysis of breast cancer tissues: Identifying differences between normal, invasive ductal carcinoma and ductal carcinoma in situ of the breast tissue. *J. Raman Spectrosc*. 38 (10): 1345–1351.
81. Haka, A. S., Volynskaya, Z., Gardecki, J. A., Nazemi, J., Lyons, J., Hicks, D., … Feld, M. S. (2006) In vivo margin assessment during partial mastectomy breast surgery using Raman spectroscopy. *Cancer Res*. 66 (6): 3317–3322.
82. Chowdary, M. V. P., Kumar, K. K., Kurien, J., Mathew, S., and Krishna, C. M. (2006) Discrimination of normal, benign, and malignant breast tissues by Raman spectroscopy. *Biopolymers* 83 (5): 556–569.
83. Yamashita, Y., Nishiumi, S., Kono, S., Takao, S., Azuma, T., and Yoshida, M. (2017) Differences in elongation of very long chain fatty acids and fatty acid metabolism between triple-negative and hormone receptor-positive breast cancer. *BMC Cancer* 17 (1): 589.
84. Ogrodzinski, M. P., Bernard, J. J., and Lunt, S. Y. (2017) Deciphering metabolic rewiring in breast cancer subtypes. *Transl. Res*. 189: 105–122.
85. Beloribi-Djefaflia, S., Vasseur, S., and Guillaumond, F. (2016) Lipid metabolic reprogramming in cancer cells. *Oncogenesis* 5 (1): e189.
86. Menendez, J. A., and Lupu, R. (2017) Fatty acid synthase regulates estrogen receptor-α signaling in breast cancer cells. *Oncogenesis* 6 (2): e299.
87. Kast, R. E., Serhatkulu, G. K., Cao, A., Pandya, A. K., Dai, H., Thakur, J. S., … Rabah, R. (2008) Raman spectroscopy can differentiate malignant tumors from normal breast tissue and detect early neoplastic changes in a mouse model. *Biopolymers* 89 (3): 235–241.
88. Surmacki, J., Brozek-Pluska, B., Kordek, R., and Abramczyk, H. (2015) The lipid-reactive oxygen species phenotype of breast cancer. Raman spectroscopy and mapping, PCA and PLSDA for invasive ductal carcinoma and invasive lobular carcinoma. Molecular tumorigenic mechanisms beyond Warburg effect. *Analyst* 140 (7): 2121–2133.
89. Surmacki, J., Musial, J., Kordek, R., and Abramczyk, H. (2013) Raman imaging at biological interfaces: Applications in breast cancer diagnosis. *Mol. Cancer* 12 (1): 48.
90. Liu, C.-H., Zhou, Y., Sun, Y., Li, J. Y., Zhou, L. X., Boydston-White, S., … Alfano, R. R. (2013) Resonance Raman and Raman spectroscopy for breast cancer detection. *Technol. Cancer Res. Treat*. 12 (4): 371–382.
91. Stone, N., Kendall, C., Smith, J., Crow, P., and Barr, H. (2004) Raman spectroscopy for identification of epithelial cancers. *Faraday Discuss*. 126: 141–157.
92. Haka, A. S., Shafer-Peltier, K. E., Fitzmaurice, M., Crowe, J., Dasari, R. R., and Feld, M. S. (2002) Identifying microcalcifications in benign and malignant breast lesions by probing differences in their chemical composition using Raman spectroscopy. *Cancer Res*. 62 (18): 5375–5380.
93. Haka, A. S., Volynskaya, Z., Gardecki, J. A., Nazemi, J., Shenk, R., Wang, N., … Feld, M. S. (2009) Diagnosing breast cancer using Raman spectroscopy: Prospective analysis. *J. Biomed. Opt*. 14 (5): 54023.
94. Abramczyk, H., Surmacki, J., Brożek-Płuska, B., Morawiec, Z., and Tazbir, M. (2009) The hallmarks of breast cancer by Raman spectroscopy. *J. Mol. Struct*. 924: 175–182.
95. Frank, C. J., McCreery, R. L., and Redd, D. C. B. (1995) Raman spectroscopy of normal and diseased human breast tissues. *Anal. Chem*. 67 (5): 777–783.
96. Abramczyk, H., Brozek-Pluska, B., Surmacki, J., Jablonska, J., and Kordek, R. (2011) The label-free Raman imaging of human breast cancer. *J. Mol. Liq*. 164 (1): 123–131.
97. Abramczyk, H., Brozek-Pluska, B., Surmacki, J., Jablonska-Gajewicz, J., and Kordek, R. (2012) Raman 'optical biopsy' of human breast cancer. *Prog. Biophys. Mol. Biol*. 108 (1): 74–81.

98. Brozek-Pluska, B., Musial, J., Kordek, R., Bailo, E., Dieing, T., and Abramczyk, H. (2012) Raman spectroscopy and imaging: Applications in human breast cancer diagnosis. *Analyst* 137 (16): 3773–3780.
99. Wang, D., and DuBois, R. N. (2007) Measurement of eicosanoids in cancer tissues. *Meth. Enzymol*. 433: 27–50.
100. Wang, D., and DuBois, R. N. (2010) Eicosanoids and cancer. *Nat. Rev. Cancer* 10 (3): 181–193.
101. Watson, M. A., Dintzis, S., Darrow, C. M., Voss, L. E., DiPersio, J., Jensen, R., and Fleming, T. P. (1999) Mammaglobin expression in primary, metastatic, and occult breast cancer. *Cancer Res*. 59 (13): 3028–3031.
102. Abramczyk, H., and Brozek-Pluska, B. (2016) New look inside human breast ducts with Raman imaging. Raman candidates as diagnostic markers for breast cancer prognosis: Mammaglobin, palmitic acid and sphingomyelin. *Anal. Chim. Acta* 909: 27–100.
103. Zhang, S., Tang, G., Russell, R. M., Mayzel, K. A., Stampfer, M. J., Willett, W. C., and Hunter, D. J. (1997) Measurement of retinoids and carotenoids in breast adipose tissue and a comparison of concentrations in breast cancer cases and control subjects. *Am. J. Clin. Nutr*. 66 (3): 626–632.
104. Pala, V., Krogh, V., Muti, P., Chajès, V., Riboli, E., Micheli, A., … Berrino, F. (2001) Erythrocyte membrane fatty acids and subsequent breast cancer: A prospective Italian study. *J. Natl. Cancer Inst*. 93 (14): 1088–1095.
105. Corsetto, P. A., Montorfano, G., Zava, S., Jovenitti, I. E., Cremona, A., Berra, B., and Rizzo, A. M. (2011) Effects of n-3 PUFAs on breast cancer cells through their incorporation in plasma membrane. *Lipids Health Dis*. 10 (1): 73.
106. Williams, C. S., Mann, M., and DuBois, R. N. (1999) The role of cyclooxygenases in inflammation, cancer, and development. *Oncogene* 18 (55): 7908–7916.
107. Thomas, G., Nguyen, T.-Q., Pence, I. J., Caldwell, B., O'Connor, M. E., Giltnane, J., … Hooks, M. (2017) Evaluating feasibility of an automated 3-dimensional scanner using Raman spectroscopy for intraoperative breast margin assessment. *Sci. Rep*. 7 (1): 13548.
108. Hanlon, E. B., Manoharan, R., Koo, T., Shafer, K. E., Motz, J. T., Fitzmaurice, M., … Feld, M. S. (2000) Prospects for in vivo Raman spectroscopy. *Phys. Med. Biol*. 45 (2): R1.
109. Motz, J. T., Gandhi, S. J., Scepanovic, O. R., Haka, A. S., Kramer, J. R., Dasari, R. R., and Feld, M. S. (2005) Real-time Raman system for in vivo disease diagnosis. *J. Biomed. Opt*. 10 (3): 31113–311137.
110. Nijssen, A., Koljenović, S., Schut, T. C. B., Caspers, P. J., and Puppels, G. J. (2009) Towards oncological application of Raman spectroscopy. *J. Biophotonics* 2 (1–2): 29–36.
111. Saha, A., Barman, I., Dingari, N. C., McGee, S., Volynskaya, Z., Galindo, L. H., … Dasari, R. R. (2011) Raman spectroscopy: A real-time tool for identifying microcalcifications during stereotactic breast core needle biopsies. *Biomed. Opt. Express* 2 (10): 2792–2803.
112. Matousek, P., and Stone, N. (2007) Prospects for the diagnosis of breast cancer by noninvasive probing of calcifications using transmission Raman spectroscopy. *J. Biomed. Opt*. 12 (2): 24008.
113. Baker, R., Matousek, P., Ronayne, K. L., Parker, A. W., Rogers, K., and Stone, N. (2007) Depth profiling of calcifications in breast tissue using picosecond Kerr-gated Raman spectroscopy. *Analyst* 132 (1): 48–53.
114. Stone, N., Baker, R., Rogers, K., Parker, A. W., and Matousek, P. (2007) Subsurface probing of calcifications with spatially offset Raman spectroscopy (SORS): Future possibilities for the diagnosis of breast cancer. *Analyst* 132 (9): 899–905.
115. Matousek, P., and Stone, N. (2009) Emerging concepts in deep Raman spectroscopy of biological tissue. *Analyst* 134 (6): 1058–1066.
116. Butler, H. J., Ashton, L., Bird, B., Cinque, G., Curtis, K., Dorney, J., … Martin-Hirsch, P. L. (2016) Using Raman spectroscopy to characterize biological materials. *Nat. Protoc*. 11 (4): 664–687.

117. Redd, D. C. B., Feng, Z. C., Yue, K. T., and Gansler, T. S. (1993) Raman spectroscopic characterization of human breast tissues: Implications for breast cancer diagnosis. *Appl. Spectrosc*. 47 (6): 787–791.
118. Depciuch, J., Kaznowska, E., Szmuc, K., Zawlik, I., Cholewa, M., Heraud, P., and Cebulski, J. (2016) Comparing paraffined and deparaffinized breast cancer tissue samples and an analysis of Raman spectroscopy and infrared methods. *Infrared Phys. Technol*. 76: 217–226.
119. Mian, S. A., Colley, H. E., Thornhill, M. H., and Rehman, I. U. (2014) Development of a dewaxing protocol for tissue-engineered models of the oral mucosa used for Raman spectroscopic analysis. *Appl. Spectrosc. Rev*. 49 (8): 614–617.
120. Gao, P., Han, B., Du, Y., Zhao, G., Yu, Z., Xu, W., … Fan, Z. (2017) The clinical application of Raman spectroscopy for breast cancer detection. *J. Spectrosc*. 2017:1–10.
121. Yu, C., Gestl, E., Eckert, K., Allara, D., and Irudayaraj, J. (2006) Characterization of human breast epithelial cells by confocal Raman micro spectroscopy. *Cancer Detect. Prev*. 30 (6): 515–522.
122. Kumar, S., Verma, T., Mukherjee, R., Ariese, F., Somasundaram, K., and Umapathy, S. (2016) Raman and infra-red microspectroscopy: Towards quantitative evaluation for clinical research by ratiometric analysis. *Chem. Soc. Rev*. 45 (7): 1879–1900.
123. Numata, Y., Otsuka, M., Yamagishi, K., and Tanaka, H. (2017) Quantitative determination of glycine, alanine, aspartic acid, glutamic acid, phenylalanine, and tryptophan by Raman spectroscopy. *Anal. Lett*. 50 (4): 651–662.
124. Han, B., Du, Y., Fu, T., Fan, Z., Xu, S., Hu, C., … Xu, W. (2017) Differences and relationships between normal and atypical ductal hyperplasia, ductal carcinoma in situ, and invasive ductal carcinoma tissues in the breast based on Raman spectroscopy. *Appl. Spectrosc*. 71 (2): 300–307.
125. Depciuch, J., Kaznowska, E., Zawlik, I., Wojnarowska, R., Cholewa, M., Heraud, P., and Cebulski, J. (2016) Application of Raman spectroscopy and infrared spectroscopy in the identification of breast cancer. *Appl. Spectrosc*. 70 (2): 251–263.
126. Li, Q. B., Wang, W., Liu, C. H., and Zhang, G. J. (2015) Discrimination of breast cancer from normal tissue with Raman spectroscopy and chemometrics. *J. Appl. Spectrosc*. 82 (3): 450–455.
127. Chaturvedi, D., Balaji, S. A., Bn, V. K., Ariese, F., Umapathy, S., and Rangarajan, A. (2016) Different phases of breast cancer cells: Raman study of immortalized, transformed, and invasive cells. *Biosensors* 6 (4):57.
128. Zheng, C., Liang, L., Xu, S., Zhang, H., Hu, C., Bi, L., … Xu, W. (2014) The use of Au@ SiO2 shell-isolated nanoparticle-enhanced Raman spectroscopy for human breast cancer detection. *Anal. Bioanal. Chem*. 406 (22): 5425–5432.
129. Rysman, E., Brusselmans, K., Scheys, K., Timmermans, L., Derua, R., Munck, S., … Swinnen, J. V. (2010) De novo lipogenesis protects cancer cells from free radicals and chemotherapeutics by promoting membrane lipid saturation. *Cancer Res*. 70 (20): 8117–8126.
130. Mariani, M. M., Maccoux, L., Matthaus, C., Diem, M., Hengstler, J., and Deckert, V. (2010) Micro-Raman detection of nuclear membrane lipid fluctuations in senescent epithelial breast cancer cells. *Anal. Chem*. 82 (10): 4259–4263.
131. Winnard Jr, P. T., Zhang, C., Vesuna, F., Kang, J. W., Garry, J., Dasari, R. R., … Raman, V. (2017) Organ-specific isogenic metastatic breast cancer cell lines exhibit distinct Raman spectral signatures and metabolomes. *Oncotarget* 8 (12): 20266.
132. Pacia, M. Z., Buczek, E., Blazejczyk, A., Gregorius, A., Wietrzyk, J., Chlopicki, S., … Kaczor, A. (2016) 3D Raman imaging of systemic endothelial dysfunction in the murine model of metastatic breast cancer. *Anal. Bioanal. Chem*. 408 (13): 3381–3387.
133. Paidi, S. K., Rizwan, A., Zheng, C., Cheng, M., Glunde, K., and Barman, I. (2017) Label-free Raman spectroscopy detects stromal adaptations in premetastatic lungs primed by breast cancer. *Cancer Res*. 77 (2): 247–256.
134. Weidner, N., Semple, J. P., Welch, W. R., and Folkman, J. (1991) Tumor angiogenesis and metastasis-correlation in invasive breast carcinoma. *N. Engl. J. Med*. 324 (1): 1–8.

135. Brozek-Pluska, B., Kopeć, M., Abramczyk, H., Zhang, C., Hazarika, P., Kelly, C., … Plass, C. (2016) Development of a new diagnostic Raman method for monitoring epigenetic modifications in the cancer cells of human breast tissue. *Anal. Methods* 8 (48): 8542–8553.
136. Wu, Y., McEwen, G. D., Harihar, S., Baker, S. M., DeWald, D. B., and Zhou, A. (2010) BRMS1 expression alters the ultrastructural, biomechanical and biochemical properties of MDA-MB-435 human breast carcinoma cells: An AFM and Raman microspectroscopy study. *Cancer Lett*. 293 (1): 82–91.
137. Giuliano, A. E., Kirgan, D. M., Guenther, J. M., and Morton, D. L. (1994) Lymphatic mapping and sentinel lymphadenectomy for breast cancer. *Ann. Surg*. 220 (3): 391.
138. Smith, J., Kendall, C., Sammon, A., Christie-Brown, J., and Stone, N. (2003) Raman spectral mapping in the assessment of axillary lymph nodes in breast cancer. *Technol. Cancer Res. Treat*. 2 (4): 327–331.
139. Hartwell, L. H., and Kastan, M. B. (1994) Cell cycle control and cancer. *Science* 266 (5192): 1821–1828.
140. Johnstone, R. W., Ruefli, A. A., and Lowe, S. W. (2002) Apoptosis: A link between cancer genetics and chemotherapy. *Cell* 108 (2): 153–164.
141. Short, K. W., Carpenter, S., Freyer, J. P., and Mourant, J. R. (2005) Raman spectroscopy detects biochemical changes due to proliferation in mammalian cell cultures. *Biophys. J*. 88 (6): 4274–4288.
142. Pichardo-Molina, J. L., Frausto-Reyes, C., Barbosa-García, O., Huerta-Franco, R., González-Trujillo, J. L., Ramírez-Alvarado, C. A., … Medina-Gutiérrez, C. (2007) Raman spectroscopy and multivariate analysis of serum samples from breast cancer patients. *Lasers Med. Sci*. 22 (4): 229–236.
143. Carter, R. A. B., Martin, A. A., Netto, M. M., and Soares, F. A. (2004) FT-Raman spectroscopy study of human breast tissue. Proceedings of Biomedical Vibrational Spectroscopy and Biohazard Detection Technologies, Biomedical Optics 2004, San Jose, California, United States, January 24–29.
144. Shashni, B., Horiguchi, Y., Kurosu, K., Furusho, H., and Nagasaki, Y. (2017) Application of surface enhanced Raman spectroscopy as a diagnostic system for hypersialylated metastatic cancers. *Biomaterials* 134: 143–153.
145. Yang, J., Wang, Z., Zong, S., Song, C., Zhang, R., and Cui, Y. (2012) Distinguishing breast cancer cells using surface-enhanced Raman scattering. *Anal. Bioanal. Chem*. 402 (3): 1093–1100.
146. Xiao, L., Harihar, S., Welch, D. R., and Zhou, A. (2014) Imaging of epidermal growth factor receptor on single breast cancer cells using surface-enhanced Raman spectroscopy. *Anal. Chim. Acta* 843: 73–82.
147. Kim, J.-H., Kim, J.-S., Choi, H., Lee, S.-M., Jun, B.-H., Yu, K.-N., … Cho, M.-H. (2006) Nanoparticle probes with surface enhanced Raman spectroscopic tags for cellular cancer targeting. *Anal. Chem*. 78 (19): 6967–6973.
148. Sha, M. Y., Xu, H., Penn, S. G., and Cromer, R. (2007) SERS nanoparticles: A new optical detection modality for cancer diagnosis. *Nanomedicine (Lond)* 2 (5): 725–734.
149. Han, X. X., Zhao, B., and Ozaki, Y. (2009) Surface-enhanced Raman scattering for protein detection. *Anal. Bioanal. Chem*. 394 (7): 1719–1727.
150. Dinish, U. S., Balasundaram, G., Chang, Y.-T., and Olivo, M. (2014) Actively targeted in vivo multiplex detection of intrinsic cancer biomarkers using biocompatible SERS nanotags. *Sci. Rep*. 4: 4075.
151. Rawal, S., Yang, Y.-P., Cote, R., and Agarwal, A. (2017) Identification and quantitation of circulating tumor cells. *Annu. Rev. Anal. Chem*. 10 (1): 321–343.
152. Xiao, L., Tian, X., Harihar, S., Li, Q., Li, L., Welch, D. R., and Zhou, A. (2017) Gd 2 O 3-doped silica@ Au nanoparticles for in vitro imaging cancer biomarkers using surface-enhanced Raman scattering. *Spectrochim. Acta Part A Mol. Biomol. Spectrosc*. 181: 218–225.

153. Allain, L. R., and Vo-Dinh, T. (2002) Surface-enhanced Raman scattering detection of the breast cancer susceptibility gene BRCA1 using a silver-coated microarray platform. *Anal. Chim. Acta* 469 (1): 149–154.
154. Vo-Dinh, T., Allain, L. R., and Stokes, D. L. (2002) Cancer gene detection using surface-enhanced Raman scattering (SERS). *J. Raman Spectrosc*. 33 (7): 511–516.
155. Wabuyele, M. B., Yan, F., and Vo-Dinh, T. (2010) Plasmonics nanoprobes: Detection of single-nucleotide polymorphisms in the breast cancer BRCA1 gene. *Anal. Bioanal. Chem*. 398 (2): 729–736.
156. Huh, Y. S., Chung, A. J., and Erickson, D. (2009) Surface enhanced Raman spectroscopy and its application to molecular and cellular analysis. *Microfluid. Nanofluidics* 6 (3): 285.
157. Pal, A., Isola, N. R., Alarie, J. P., Stokes, D. L., and Vo-Dinh, T. (2006) Synthesis and characterization of SERS gene probe for BRCA-1 (breast cancer). *Faraday Discuss*. 132: 293–301.
158. Manciu, F. S., Ciubuc, J. D., Parra, K., Manciu, M., Bennet, K. E., Valenzuela, P., … Francia, G. (2017) Label-free Raman imaging to monitor breast tumor signatures. *Technol. Cancer Res. Treat*. 16 (4): 461–469.
159. Vargas-Obieta, E., Martínez-Espinosa, J. C., Martínez-Zerega, B. E., Jave-Suárez, L. F., Aguilar-Lemarroy, A., and González-Solís, J. L. (2016) Breast cancer detection based on serum sample surface enhanced Raman spectroscopy. *Lasers Med. Sci*. 31 (7): 1317–1324.
160. Abramczyk, H., Brozek-Pluska, B., Surmacki, J., Musial, J., and Kordek, R. (2014) Oncologic photodynamic diagnosis and therapy: Confocal Raman/fluorescence imaging of metal phthalocyanines in human breast cancer tissue in vitro. *Analyst* 139 (21): 5547–5559.
161. Rae, A., Stosch, R., Klapetek, P., Walker, A. R. H., and Roy, D. (2014) State of the art Raman techniques for biological applications. *Methods* 68 (2): 338–347.
162. Driscoll, A. J., Harpster, M. H., and Johnson, P. A. (2013) The development of surface-enhanced Raman scattering as a detection modality for portable in vitro diagnostics: Progress and challenges. *Phys. Chem. Chem. Phys*. 15 (47): 20415–20433.
163. Carey, P. R. (1999) Raman spectroscopy, the sleeping giant in structural biology, awakes. *J. Biol. Chem*. 274 (38): 26625–26628.